

DEVELOPMENT OF SECONDARY FAULTS BETWEEN EN ECHELON,
OBLIQUE-SLIP FAULTS: EXAMPLES FROM BASEMENT CONTROLLED,
SMALL-FAULT SYSTEMS IN THE LLANO UPLIFT OF CENTRAL TEXAS

A Thesis

by

HOWARD REIFFERT HEDGCOXE

Submitted to the Graduate College of
Texas A&M University
in partial fulfilment of the requirements for the degree of

MASTER OF SCIENCE

August 1987

Major Subject: Geology


DEVELOPMENT OF SECONDARY FAULTS BETWEEN EN ECHELON,
OBLIQUE-SLIP FAULTS: EXAMPLES FROM BASEMENT CONTROLLED,
SMALL-FAULT SYSTEMS IN THE LLANO UPLIFT OF CENTRAL TEXAS

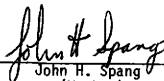
A Thesis

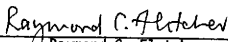
by

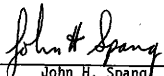
HOWARD REIFFERT HEDGCOXE

Approved as to style and content by:


Brand Johnson
(Chairman of Committee)


John H. Spang
(Member)


Raymond C. Fletcher
(Member)


John H. Spang
(Head of Department)

August 1987

ABSTRACT

Development of Secondary Faults Formed En Echelon, Oblique-Slip
Faults: Examples From Basement Controlled, Small-Fault Systems
in the Llano Uplift of Central Texas (August 1987)

Howard Reiffert Hedgcoxe, B.S., Texas A&M University

Chair of Advisory Committee: Dr. Brann Johnson

Reactivation of discontinuities within the Precambrian basement of the Llano region during the Ouachita Orogeny, influenced the nature of deformation in the overlying Paleozoic sediments. This influence is readily observed in outcrops of the lower 2-10 m of the basal Cambrian Hickory Sandstone, exposed along the Llano river in Mason County, Texas. Numerous fault systems, defined by fault type, timing, distribution and orientation are often observed in the same outcrop. The number and orientations of fault systems varies throughout the study area and correspond to fracture trends in adjacent basement outcrops. Fractures in the sandstone post-date but commonly are associated spatially with faults. Movements in the underlying basement are inferred to control the heterogeneous deformation in the sandstone.

Detailed mapping of an outcrop of Hickory Sandstone situated, 2-4 m above the basement, documents a distinctive, scale independent, fault-zone geometry associated with interaction between en echelon, oblique-slip faults. The Elementary geometry is characterized by a

pair of overlapping, primary faults that step opposite to their sense of shear, and a system of secondary antithetic faults restricted between and oriented oblique to the bounding faults. With increasing displacement on the bounding faults, the system of secondary faults evolves from an Elementary to a Compound, to an Advanced geometry, which includes the formation of secondary synthetic faults and sub-systems of higher order antithetic faults. Synthetic faults have the same sense of shear, are subparallel to the primary faults, and usually cut early formed antithetic faults, which have an opposite sense of shear relative to the primary faults. Synthetic faults form interior to and ahead of the bounding faults, increasing the effective overlap.

Displacements on antithetic faults are directly related to changes in displacement on associated bounding faults. Additionally, markers provide information on the distribution of displacement within and outside the overlap region. This evidence leads to the interpretation that the secondary faults mechanically link the bounding faults, permitting displacement transfer through the overlap region.

ACKNOWLEDGEMENTS

First and foremost, I wish to acknowledge the support and encouragement that I received from my mother and father and my wife, Anne during my long career at Texas A&M. I especially want to thank Dr. Pat G. Hedgcoxe for instilling in me the desire to learn and to understand the physical world. Then, I want to thank my friend and mentor, Dr. Brann Johnson who, throughout my undergraduate and graduate careers, played a key role in my development as a person and a scientist. The satisfaction I achieved from my thesis and appreciation for the field work was greatly enhanced because of Brann Johnson's willingness to tackle new problems and because of his enthusiasm in sharing in the learning experience. Committee member and undergraduate advisor, Dr. John Spang, helped to foster my interest in structural geology. My other committee member, Dr. Ray Fletcher, always kept an open door and provided important insights into the problems of fault interactions.

I also want to acknowledge the work and special friendship of my contemporaries, Joe Becker who pioneered the structural problems of the Western Llano Uplift and Mark Schmittle who shared many hot days and late nights in the field, thanks for helping to keep things out of control; to my office mates who shared and suffered through the last days of the Bull Pen: Jim Evans, Pete Hennings, Ted Hopkins, Frank Irwin, Ed Juddo, Dave Kraig, Ned Mamula, Duncan Mardon, Dave McConnell, Ken Wilks, and the Chesters, and to other more recent

Tectonophysicists: Russ Davies, Doug Goff, Bill Kilsdonk, and Bill Shea, thanks for helping to maintain the proper degree of insanity while working on the cutting edge. Special thanks to Dr. Robert Berg for the raquetball lessons.

The hospitality of the people of Mason County and Mr. and Mrs. Jack Walker in particular is greatly appreciated. Financial support for the field work was provided, in part, by the Geology Department at Texas A&M University, by the Center for Tectonophysics, by a fellowship from Chevron Oil Company and by a thesis research grant from the Gulf Coast Section Society of Economic Paleontologists and Mineralogists. Robin McNeely artfully interpreted my handwriting and typed the text of the thesis.

TABLE OF CONTENTS

	PAGE
ABSTRACT.....	iii
ACKNOWLEDGMENTS.....	v
TABLE OF CONTENTS.....	vii
LIST OF FIGURES.....	ix
LIST OF PLATES.....	xii
CHAPTER I. INTRODUCTION.....	1
Definition of Problem and Objectives.....	1
Method of Investigation.....	3
Regional Geologic Setting.....	3
Stratigraphy.....	4
Structure.....	6
Normal Faults.....	6
Syncline.....	8
CHAPTER II. LOCAL STRUCTURAL SETTING AND DETAILED STUDY OF FAULT SYSTEMS WITHIN AN OUTCROP.....	10
Structural Elements.....	12
Fractures.....	12
Small Faults.....	14
Large Faults.....	14
Fracture Trends in the Basement and Fault Trends in the Sandstone.....	16
Interrelations of Faults and Fractures Developed in an Outcrop.....	21
Fault Systems.....	21
System 1.....	21
System 2.....	23
System 3.....	23
System 4.....	26
System 5.....	30
Main Fault.....	33
Fault System Relationships.....	36
Fracture Sets.....	37
Set 1.....	40
Set 2.....	40
Set 3.....	40
Set 4.....	41

TABLE OF CONTENTS (continued)

	PAGE
Discussion: Kinematic Model of Faulting in the Outcrop...	41
CHAPTER III. CHARACTERISTICS OF SECONDARY FAULT ZONES BETWEEN EN ECHELON, INTERACTING OBLIQUE SLIP FAULTS.....	49
Geometry of Secondary-Fault Zones.....	51
Dimensions of Secondary-Fault Zones.....	56
Characteristics of Secondary Faults.....	60
Antithetic Faults.....	60
Synthetic Faults.....	63
Intersections Between Antithetic and Synthetic Faults....	68
Evolution of a Compound Secondary-Fault Zone.....	70
Stage 1.....	71
Stage 2.....	71
Stage 3.....	73
Stage 4.....	73
Displacements.....	76
Interpretation.....	85
CHAPTER IV. DISCUSSION: RELATION TO PREVIOUS WORK AND EVOLUTION OF A TYPICAL SECONDARY-FAULT ZONE.....	86
CHAPTER V. CONCLUSIONS AND MODEL OF SECONDARY-FAULT ZONE EVOLUTION.....	100
REFERENCES CITED.....	107
VITA.....	110

LIST OF FIGURES

FIGURE	PAGE
1. Regional geology of the southwestern part of the Llano Uplift, Mason County, Texas.....	5
2. Major structural features of the area south of Mason, Texas.....	7
3. Geologic map of the study area.....	11
4. A typical fracture and a single small fault in the Hickory Sandstone.....	15
5. Fracture attitudes measured in basement outcrops in the study area.....	17
6. Fracture attitudes measured in basement outcrops and small fault attitudes in sandstone outcrops in the study area.....	19
7. Oblique view of Llano River outcrop of Hickory Sandstone.....	22
8. Distribution of members of System 1 and System 2 faults in the Llano River outcrop.....	25
9. Distribution of fault system 1, 2, 3 and 4 and early-formed elements of System 5 faults in the Llano River outcrop.....	28
10. Detachment and thrust faults of System 4.....	29
11. Distribution of faults in the Llano River outcrop.....	32
12. Map of System 5 faults showing the Main Fault and location of fault System 2 and System 3.....	35
13. Distribution of faults and fracture Sets 1, 2, 3 and 4 in the Llano River outcrop.....	39
14. Kinematic model of fault development in the Llano River outcrop.....	45
15. Schematic illustration of an Elementary Secondary-Fault Zone.....	50

LIST OF FIGURES (continued)

FIGURE	PAGE
16. Schematic illustration of a Compound Secondary-Fault Zone.....	54
17. Example of a simple compound SFZ.....	55
18. Map of the Central SFZ, an example of a complex Compound SFZ.....	57
19. Log-log plot of initial overlap (P) and effective overlap (L) versus spacing (W) of primary faults from SFZ in the Llano River outcrop.....	59
20. Frequency plot of values of α	62
21. Types of synthetic faults.....	64
22. Detailed map of part of the Central SFZ.....	66
23. Types of secondary fault intersections.....	67
24. Evolution of the Central SFZ.....	72
25. Example of an Advanced SFZ.....	75
26. Detail of marker faults offset near an antithetic/primary fault intersection.....	77
27. Detailed map of a portion of the lower part of the Central SFZ.....	81
28. Detailed map of a SFZ with left-stepping, right-lateral bounding faults.....	84
29. (A) Map of fault zone exposed in cross-section in a South African gold mine.....	87
30. Model of interacting shear cracks in a linearly elastic isotropic material.....	90
31. Line drawing of a SFZ developed in a migmatite experimentally deformed at 1 Kbar, 150°C and strain rate of 1% per minute.....	96

LIST OF FIGURES (continued)

FIGURE	PAGE
32. Comparison of Riedel shear array to the Elementary SFZ geometry.....	98
33. Generalized model of Secondary-Fault Zone evolution....	104

LIST OF PLATES

PLATE (in back pocket)

1. Map of fractures and small faults developed in an outcrop of Hickory Sandstone exposed along the Llano River, Mason County, Texas.

CHAPTER I

INTRODUCTION

Definition of Problem and Objectives

Detailed mapping shows that, in their incipient stage, fault zones consist of en echelon arrays of individual faults (Becker, 1985; Gay and Ortlepp, 1979; Tchalenko, 1970; Wilcox et al., 1973). With increasing displacement, deformation processes at ends of the early formed faults control the evolution of the fault zone. Therefore, understanding fault-fault interaction is a fundamental problem of structural geology.

Fault zones formed by interaction between overlapping en echelon, strike-slip dominant faults are well-exposed in outcrops of Cambrian sandstone along the Llano River in Mason County, Texas. Later formed (secondary) faults are restricted to the overlap region between early-formed (primary) fault pairs, forming a distinctive fault zone configuration. This configuration is developed consistently over a wide range of scales. The principal objective of this study is to document the geometric, temporal and kinematic relationships between the primary faults and the associated secondary faults and to provide insight into the mechanics of interaction between en echelon faults in a porous sandstone.

Recent field investigations of large-displacement normal faults in the Llano Uplift of central Texas (Becker, 1985; Johnson and

This thesis follows the style of the Geological Society of America Bulletin.

Becker, 1986) indicate that deformation in the overlying sediments is influenced by faults and fractures in the Precambrian basement. Therefore, an additional objective of this study is to determine the role of basement control on the development of the faults and fractures in the overlying sandstone. This associated study provides an understanding of the conditions under which the system of en echelon faults developed.

This study is presented in two parts. Part I is presented in Chapter II, which focuses on the local structural setting of the faulted sandstones. The relationship between structures in the basement and the overlying sediments is established by: 1) identifying and comparing fracture trends in the basement to small-fault trends in the sandstones, and 2) detailed mapping of an outcrop that is situated approximately 2-4m above basement. The outcrop exhibits several fault systems, including a system of interacting en echelon faults and associated secondary-fault zones.

Part II, Chapter III is concerned with the general characteristics of the secondary-fault zones and investigates the relationship between the secondary and primary faults. This provides the basis for an interpretation of the mechanical role of secondary faulting between en echelon fault segments. Discussion of the secondary-fault zones (Chapter IV) includes examples of similar features described in other field and laboratory studies. In addition, results from existing mechanical analyses are presented to provide additional insight into the mechanics of the observed secondary faults. The secondary-fault zones are interpreted to form due to fault interaction and allow

displacement transfer from one primary fault to the other. A model of the evolution of fault zones is presented, which is based on the field relationships and interpretation of displacement transfer.

Method of Investigation

The study involved two levels of detailed mapping. Geologic mapping, with emphasis on the fractures and small faults in the field area, was conducted at a scale of $\sim 1:4800$ on an aerial photo base map. Attitudes of fractures and small faults were recorded and plotted in order to observe structural trends within the field area. In some cases, the number of features in an outcrop was small, so that all were measured; however, in most cases, only representative attitudes were recorded.

A second level of more detailed mapping, at scales of 1:120 to 1:30 and larger, was conducted in order to facilitate the study of fault zone characteristics. This level of mapping, which focused on a single outcrop of Hickory Sandstone, used a modified pace and compass method and a portable grid, in order to accurately record the location of structures in the outcrop. In some cases photographs of the outcrop were used as base maps, allowing accurate representation of fault zone configuration in complexly faulted areas.

Regional Geologic Setting

The Llano Uplift is a broad structural dome that exposes a core of Precambrian igneous and metamorphic basement, which is flanked by a

~1000 m thick sequence of Paleozoic (mid-Cambrian to Pennsylvanian) clastics and carbonates (Figure 1). The Uplift is characterized by a system of segmented, N to NE trending, normal faults that developed as a result of lithospheric plate flexure associated with continental convergence during the Pennsylvanian Ouachita Orogeny (Becker, 1985). The study area is situated within the southwestern part of the Llano Uplift, approximately 16 km southeast of the town of Mason, Mason County, Texas (Figure 1).

Stratigraphy

The oldest unit exposed in the area is the Packsaddle schist, which is composed of various rock types. Within the study area, the Packsaddle is predominantly a biotite hornblende schist and gneiss. The Packsaddle is intruded by several large granitic bodies. The oldest intrusion in the Western Llano Uplift, the Town Mountain Granite, is a coarse grained, quartz-plagioclase-microcline granite. Slightly younger, finer grained and less mafic granite bodies are often associated with the boundaries of the Town Mountain Granite.

The Precambrian basement is overlain by the middle to upper Cambrian rocks of the Riley Formation. The Riley Formation, which includes the basal Hickory Sandstone member, is a sequence of transgressive sandstones and sandy limestones.

The overlying Wilburns Formation and Ordovician Ellenburger Group rocks represent a second transgression that is dominated by carbonate

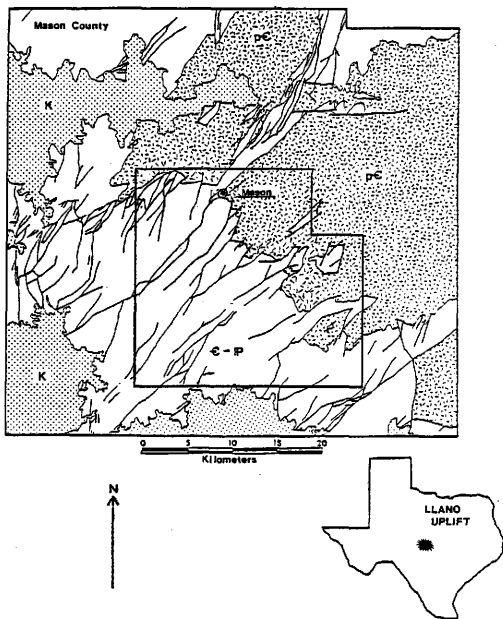


Figure 1. Regional geology of the southwestern part of the Llano Uplift, Mason County, Texas. Outlined area shown in greater detail in Figure 2. Precambrian basement rocks are indicated by pC, Cambrian to Pennsylvanian sediments by C - P and Cretaceous sediments by K.

deposition. A regional, low angle, unconformity separates the Ellenburger Group from the overlying Devonian and Mississippian shales and carbonates. This unconformity reflects a broad, low amplitude pre-Devonian uplift, centered WNW of the Llano region, along the Concho Arch (Cheney and Goss, 1952). Shales and interbedded limestones of the Pennsylvanian Marble Falls and Smithwick Formation are the youngest Paleozoic rocks exposed in the area and are syndepositional with faulting. Becker (1985) provides a summary of the geologic history of the area that emphasizes the development of Paleozoic deformation.

Structure

The structural geology of the area is dominated by two major structural features: 1) a system of regional N to NE trending normal faults and 2) a large, low amplitude, NW trending, SE plunging syncline (Figure 2). Aspects of these features are related to the NW trending contact between granitic and metamorphic basement. The inferred boundaries between the Town Mountain plutons and the Packsaddle Schist and the younger Precambrian granites (Figure 2) are interpreted from both geophysical (Andreason and Petrafeso, 1963) and limited outcrop data.

Normal Faults. The segmented nature of the faults in the Llano uplift (Figure 2) occurs at a range of scales (Becker, 1985; Schmittle, 1987) and is typical of the deformational style of the uplift. While the dominant motion on the faults is dip slip, locally, oblique-slip is required by the lateral variation of fault throw and

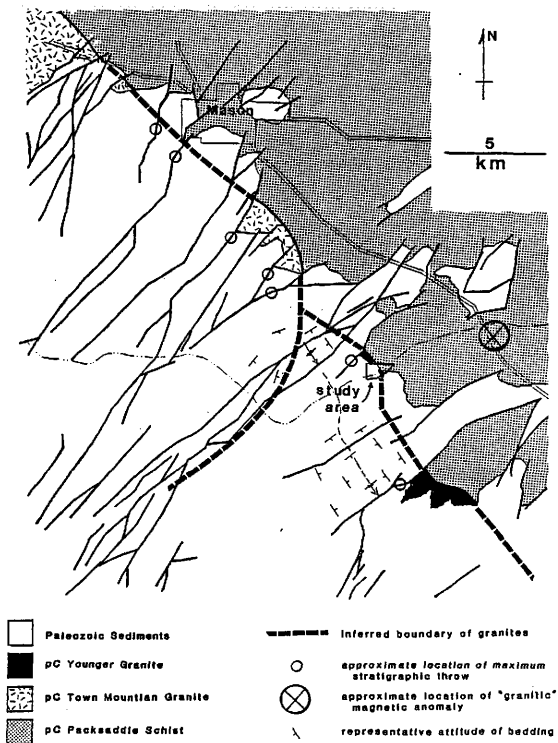


Figure 2. Major structural features of the area south of Mason, Texas.

fault orientations that are oblique to regional extension. Indications of oblique-slip in the form of inclined slickensides also has been reported (Schmittle, 1987 and Johnson, pers. comm.).

Becker (1985) and Johnson and Becker (1986) contend that the style and distribution of deformation is closely tied to basement lithology:

1) large-displacement discrete faults localize within the granites and tend to lose displacement and splay into smaller, more distributed faults in the metamorphic terrain (Figure 2);

2) several of the faults have a more northerly trend where they cross from granitic into metamorphic basement. To the west of the field area, the faults have a more easterly trend (Figure 2). Aeromagnetic and gravity data suggest that a body with granite-like characteristics may underlie this area;

3) the maximum separation on the large-displacement faults is located just to the west of and follows the known and inferred Precambrian granite/ metamorphic basement contact (Figure 2).

Syncline. With the exception of local drag folds associated with faulting, folding in the Paleozoics is not a major mechanism of deformation in the Llano uplift. However, previous investigators (Wilson, 1957; Fisher, 1960; Schmittle, 1987) have mapped a broad, low amplitude syncline trending nearly perpendicular to regional faults (Figure 2).

Changes in bedding attitude associated with the fold show a relationship to the granitic/metamorphic contact. Regionally, bedding

dips gently to the southeast. In the northern portion of the syncline, dips range from $\sim 2-5^\circ$ SW on the east side of the syncline, increasing to $\sim 6-9^\circ$ (and as high as 18) SSW near the nose region, then gradually swing to SE ($\sim 4-6^\circ$) on the west limb. Bedding attitudes of limestones higher in the section indicate that the change in strike from the east limb to the nose is fairly sharp and that the change back to regional dip is more gradual along the south west limb (Fisher, 1960; Wilson, 1957; Schmittle, 1987). This sharp change is nearly coincident with the inferred contact between the younger granite and metamorphic basement. The axial trace of the syncline appears to be offset across the Llano river. This "offset" is coincident with an easterly swing in the projected contact between the granitic and the metamorphic basement. In addition, the axial trace of the syncline is colinear with the trend of maximum separation of the normal faults (Figure 2).

These observations indicate that differences in the mechanical response of the basement rocks to the brittle deformation associated with uplift had a measurable influence on the development of large-scale structures in the overlying Paleozoic sediments.

CHAPTER II

LOCAL STRUCTURAL SETTING AND DETAILED STUDY OF
FAULT SYSTEMS WITHIN AN OUTCROP

The field area is situated along the north bank of the Llano river on the eastern limb of the syncline (Figure 2). Bedding in the area dips $\sim 2-4^\circ$ SW. Within the area, the lower 2-10 m of the basal Hickory Sandstone is exposed above the Precambrian basement. The sandstone is underlain by fine grained granite in the west and hornblend-gneiss in the east (Figure 3). Foliation in the Packsaddle Schist is steeply dipping and trends NW. Fractures paralleling foliation were not observed in the field area, thus, it is not a prominent plane of weakness and appears not to have influenced fault development during the Pennsylvanian deformation.

The contact between the gneiss and granite is covered throughout most of the area, but usually, it can be located to within a few meters and is thought to be fairly sharp. With the exception of pegmatite and aplite veins, the granite is relatively homogeneous and has no strong flow foliation. Local relief on the upper basement surface is estimated to be not more than 10-20 m. Small monadnocks of granite and gneiss are present in the field area (Figure 3). The depositional contact between the Hickory Sandstone and Precambrian basement is exposed in several places within the field area. Locally, there is no evidence for a Cambrian weathering horizon on the Precambrian basement.

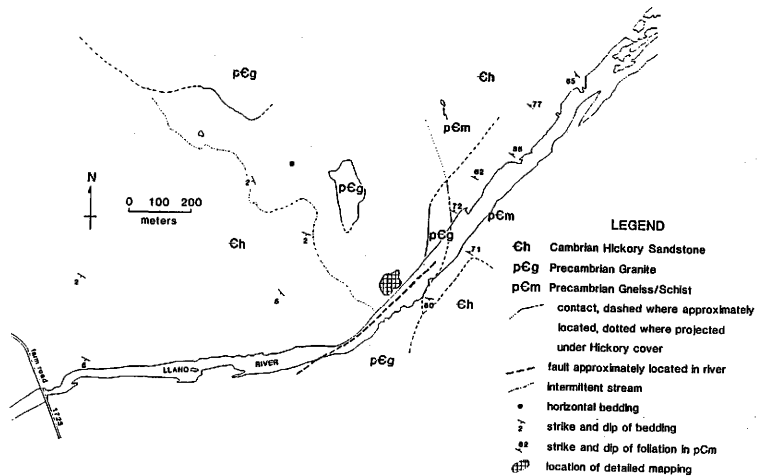


Figure 3. Geologic map of the study area

The Hickory Sandstone is generally divided into three units (Barnes and Bell, 1977; Schmittle, 1987). This study focuses on deformation in the lower unit, which is a high porosity, generally coarse grained, poorly to moderately-well cemented, poorly-sorted sandstone with some silty interbeds. Individual bed sets may be up to 1-2 m thick but generally lack extensive lateral continuity. Regionally, the lower Hickory is regarded as a relatively clean quartzose sandstone. Within lower bed-sets, in the study area, the sandstone contains significant potassium feldspar. Conglomeratic horizons composed of large, often euhedral crystals and angular grains of quartz and K-spar are common near the basement/sandstone contact. The surfaces between bed-sets usually are sharp. Sedimentary structures within the bed-sets range from ripples to trough crossbeds. Changes in grain size imparts a strength anisotropy to the sandstone.

Structural Elements

Field mapping reveals that deformation in the study area is manifest primarily as fractures and small faults. Folding is not observed and only one fault with displacement greater than 1 m is identified within the study area.

Fractures

Individual fractures occur as planar or curvilinear surfaces of separation. A fracture trace may be continuous throughout its length or it may be composed of very closely spaced en echelon segments.

Most fractures are members of a distinct set. Multiple fracture sets typify most outcrops.

Within fresh outcrops of crystalline basement, fractures have sharply defined surfaces with no gouge material observed. Some fractures in the basement have shear displacements on the order of a few millimeters. Fracture density, within the metamorphic basement, is sensitive to lithology, although, fracture spacings are not uniform in any given basement rock type. The age of fractures in the basement in the field area is not definitively known. Studies in other parts of the Llano uplift have documented several stages of pre-Pennsylvanian fracturing, much of which has a Precambrian origin (Boyer et al., 1964; Groshong, 1967; Hutchinson, 1956; and Iranpanah, 1964). A few mineral-filled fractures, suggesting a Precambrian age, were observed in the field area.

Fractures in the Hickory Sandstone are usually open with no gouge occurring between the surfaces. Liesegang bands of iron-oxide staining are commonly associated with one or both sides of the fracture, indicating that they have been conduits to fluid flow (Figure 4). In contrast to basement fractures, fractures in the sandstone exhibit no shear displacement and are interpreted to form in extension with displacement normal to the surface. In all cases, fractures in the sandstone post-date fault development in the sandstone.

EAh fractures = joint

Small Faults

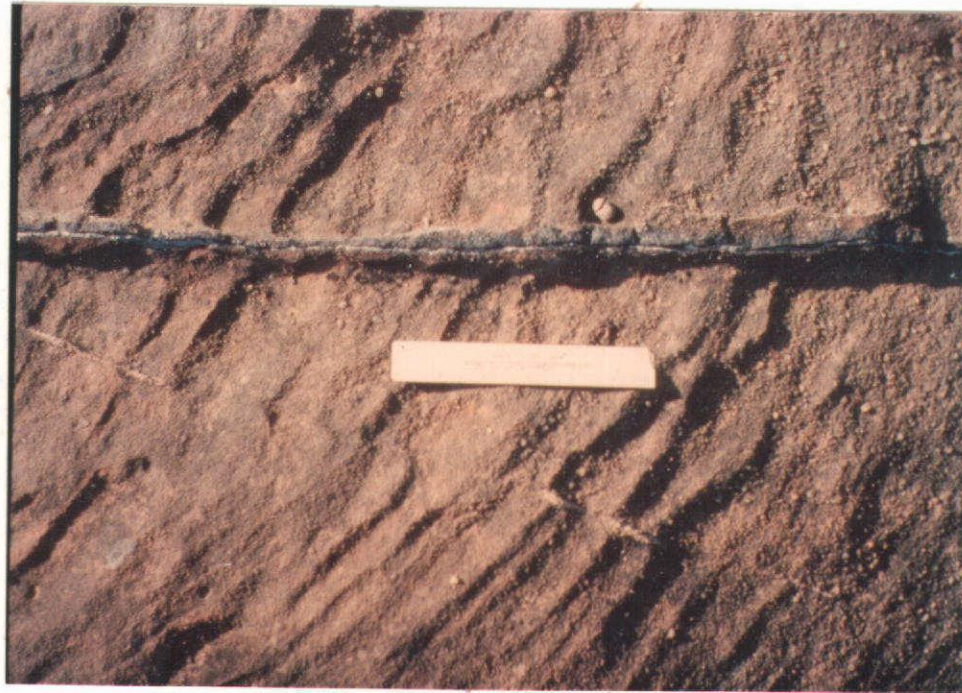
Small faults in the sandstones occur as prominent "bands" of gouge that are lighter in color than the host-rock. The gouge material is more resistant to weathering so that the faults often stand out in relief on the outcrop. Small faults in the Hickory are similar to faults formed in other porous sandstones (Aydin, 1978; Young, 1982; Heald, 1956; Pittman, 1981; Jamison, 1979; and Schmittle, 1987). Shear displacements of less than 1 mm can generate clearly discernable gouge so that small faults are easily distinguished from fractures with no shear offset (Figure 4). In addition, small faults with greater amounts of displacement have thicker gouge and sometime have a braided or ropey appearance. This relationship is used to establish relative magnitudes of displacement on small faults where independent evidence, such as offset markers are absent.

Shapes of fault traces vary from straight to highly curved or sigmoidal and are partly a function of view relative to the displacement vector. In plan view, strike-slip dominant faults have straighter traces than dip-slip dominant faults.

Large Faults

Only one fault with displacement greater than 1 m is present in the study area. It is located in the Llano river where the river channel changes from nearly east-west to about N50E, parallel to the regional fault trend. The sense and amount of offset on the fault is not known, however, the sandstone/basement contact is approximately

single small fault



fracture

Figure 4. A typical fracture and a single small fault in the Hickory Sandstone. Note small offset of crossbedding by the small fault.

8-10 m higher on the southeast side of the river than on the northwest side. Assuming that the upper basement surface is planar, as much as 8-10 m of dip-slip movement down to the NW is possible. A component of strike-slip cannot be ruled out, but the field data is inadequate to constrain an estimate. This fault was not observed within outcrops of the Packsaddle to the east, so it either dies out as a distributed zone of fracturing or it lies totally within the river.

Fracture Trends in the Basement and Fault Trends in the Sandstone

Data obtained from granite and metamorphic outcrops show that basement fractures, at any given location, have diverse attitudes. The two most commonly occurring fracture attitudes strike generally northeast and northwest, but as few as one or as many as five fracture sets may be observed within any given outcrop (Figure 5). The fracture orientations in the basement exhibit significant spatial variations within the field area. For example, a north trending fracture set occurs in basement outcrops near the granite/gneiss contact north of the river (Figure 5). This fracture set is not observed in granite outcrops to the west and is observed in the gneiss for only about 200 m eastward. The fact that this fracture set is best developed near the granite/gneiss contact, and that the contact is also north trending, suggests that the fracture set and the granite/gneiss contact are related. Another significant spatial difference is observed by noting the well-developed NW and WNW fracture trends in basement outcrops in

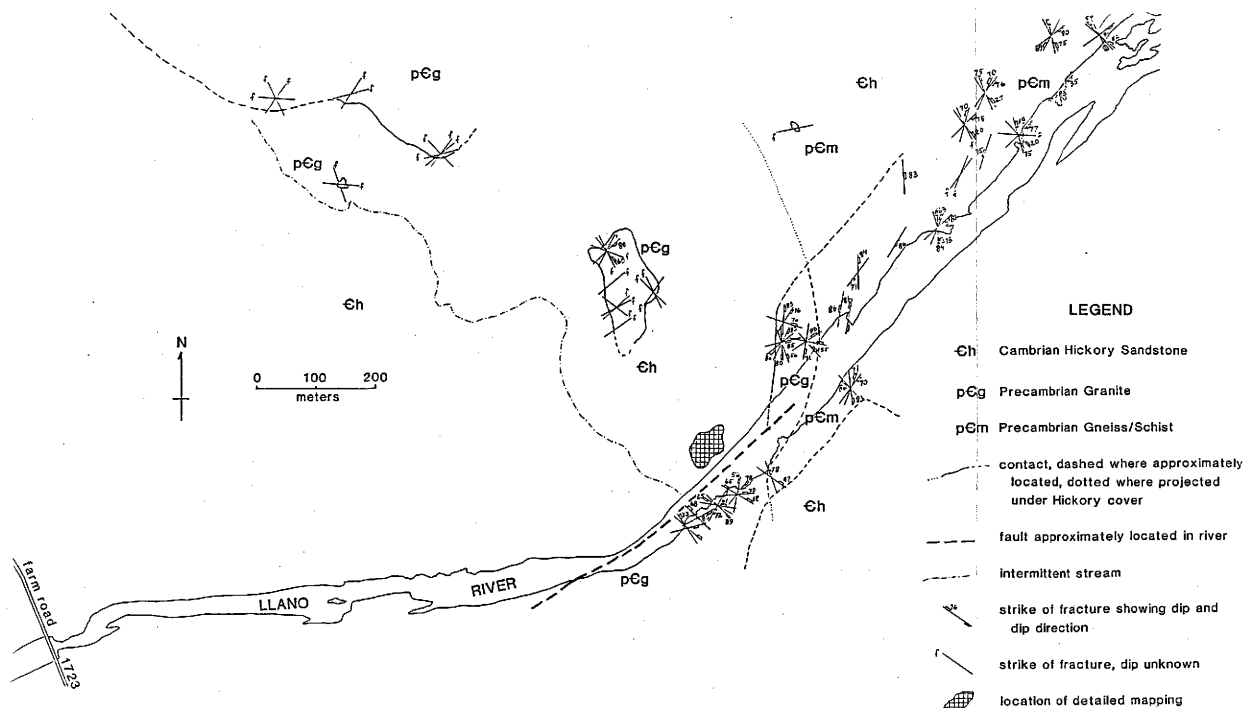


Figure 5. Fracture attitudes measured in basement outcrops in the study area.

the western two-thirds of the field area. These fracture sets are only weakly-developed or absent in outcrops of gneiss in the east (Figure 5).

Comparing fracture data from granite outcrops with small fault data in adjacent sandstone outcrops, reveals that attitudes of small faults in the sandstone commonly correspond to fracture sets in the underlying basement. For example, the NE and NW small-fault trends in the sandstone outcrops along the stream (Figure 6, rose H₂) correspond to fracture orientations in the nearby granite outcrops (Figure 6, rose G₂). In addition, a set of north trending small faults in sandstone outcrops near the sandstone/granite contact, along the north bank of the river (Figure 6, rose H₄), closely correlates to the previously mentioned north trending set of basement fractures, which appears related to the granite/gneiss contact (Figure 6, rose G₃).

Fracture trends in the basement do not always have corresponding small-fault trends in the sandstone. For example, returning to the rose diagrams at locations G₃ and H₄, the NE and WNW fracture trends at G₃ are not mirrored by small-fault trends at H₄ (Figure 6). Further study of attitudes in the outcrops north of the river, near the granite/gneiss contact shows that fault trends can develop without a corresponding fracture set. Note, in particular, the set of low angle, NW trending faults in the sandstone outcrops (Figure 6, rose H₄). No shallow dipping fractures were observed in the adjacent granite outcrops.

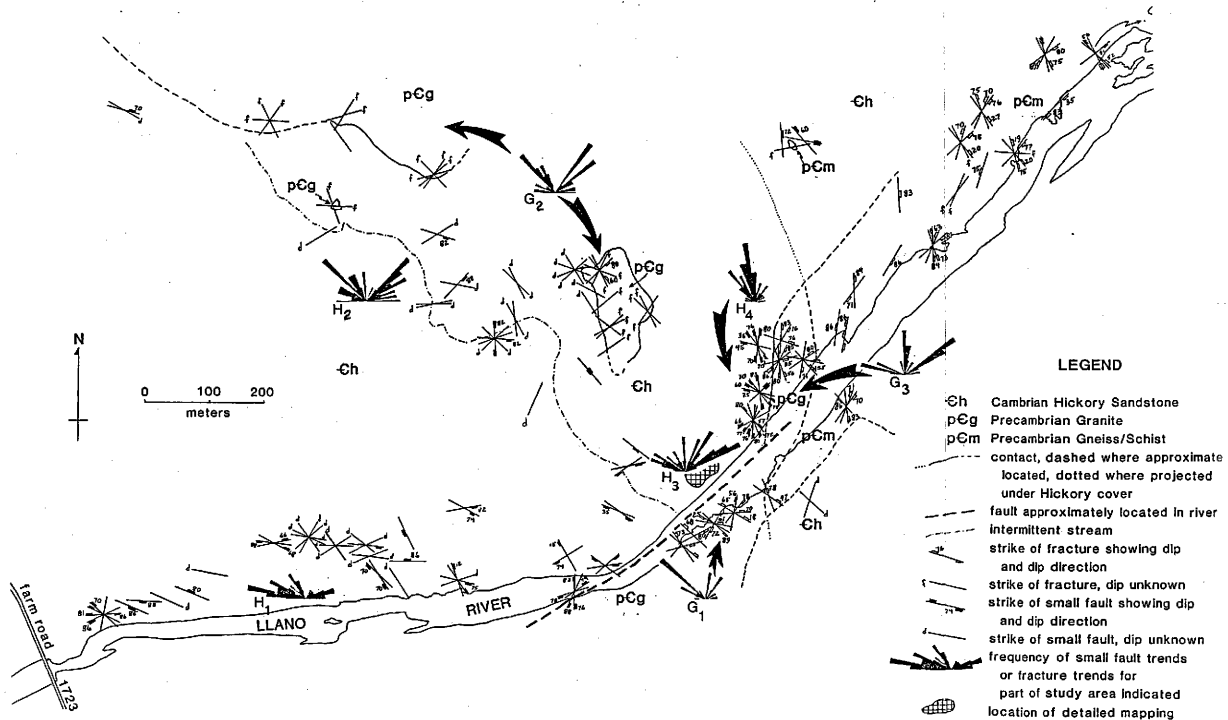


Figure 6. Fracture attitudes measured in basement outcrops and small fault attitudes in sandstone outcrops in the study area.

Fault trends in the Hickory Sandstone exhibit significant variations across the field area. For example, a prominent WNW small-fault trend is observed in sandstone outcrops in the southwestern and south-central part of the field area (Figure 6, rose H_1 and H_3). However, outcrops to the north, represented by rose diagrams at H_2 and particularly at H_4 , do not have a strongly developed WNW fault trend. Also, the N40-60E fault trend that is observed at locations H_2 and H_3 is essentially absent in sandstone outcrops in the southwest (Figure 6, rose H_1). It is interesting to note that fractures oriented WNW and NW are observed in basement outcrops at locations G_1 and G_2 . However, a clear relationship between structural trends in the basement and overlying sediment in the western part of the field area cannot be established due to limited outcrop.

In addition to variations in attitudes, small faults in the study area exhibit varying senses of shear. Both high and low angle faults with normal and reverse slip as well as strike-slip dominant faults are often developed within the same outcrop. Faults within any given outcrop also have systematic age and spatial relationships, allowing the identification of distinct fault systems. Field relations do not indicate that the faulting in the sandstone represents more than one major period of deformation.

From a mechanics standpoint, movement along surfaces of weakness, in the form of pre-existing fractures, in the basement is a reasonable model to explain the origin of the diverse trends and senses of movement of faults in the overlying sandstone. The distribution and

orientation of reactivated basement fractures controls the heterogeneity of deformation of the sandstones observed in the field area.

Interrelations of Fault and Fracture Systems Developed in an Outcrop

The major portion of the field work involved detailed mapping and investigation of faults and fractures developed within a 50 x 70 m outcrop of Hickory Sandstone, situated approximately 2-4 m above the sandstone/basement contact (Figure 7). The outcrop lies within the flood plain of the Llano River, which helps to keep the sandstone uncharacteristically well exposed. The rose diagram at location H₃ in Figure 6 shows that numerous fault trends are present in the outcrop.

Fault and fracture development is not uniform through out the outcrop. Some areas in the outcrop exhibit a high density of faults, whereas others are essentially free of deformation (Plate 1). Five fault systems and four fracture sets occur within the outcrop. The following description and discussion of the systems is presented sequentially from oldest to youngest, providing a scenario of structural development of the outcrop. Each of the structural systems are defined on the basis of timing, attitude, distribution (location, spacing and length), sense of slip and amount of offset of the members that compose the systems.

Fault Systems

System 1. The oldest fault system in the outcrop consists of steeply dipping, N to NNW trending faults, some of which form a poorly



Figure 7. Oblique view of Llano River outcrop of Hickory Sandstone. Detailed mapping (1:120) covered eastern 2/3 of outcrop. View is toward the northwest, hills in background are resistant Cambrian carbonates exposed in the axial part of the syncline.



Figure 7. Oblique view of Llano River outcrop of Hickory Sandstone. Detailed mapping (1:120) covered eastern 2/3 of outcrop. View is toward the northwest, hills in background are resistant Cambrian carbonates exposed in the axial part of the syncline.



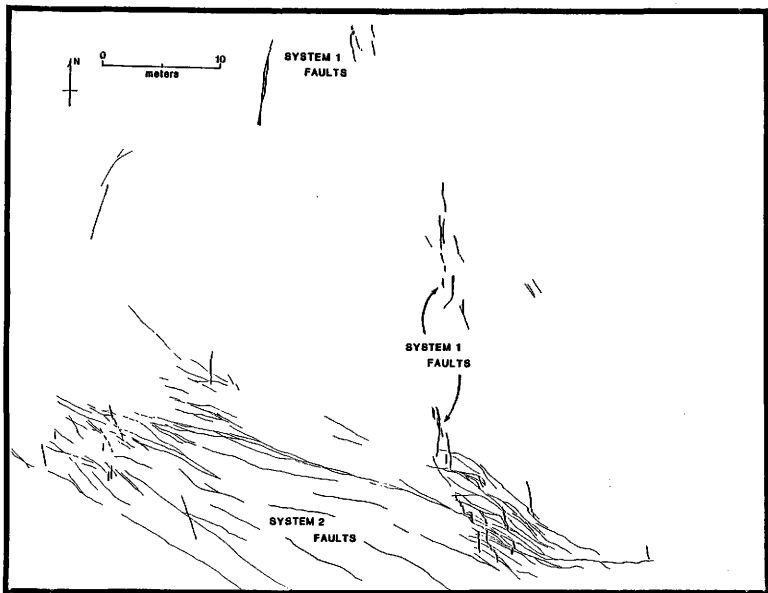
Figure 7. Oblique view of Llano River outcrop of Hickory Sandstone. Detailed mapping (1:120) covered eastern 2/3 of outcrop. View is toward the northwest, hills in background are resistant Cambrian carbonates exposed in the axial part of the syncline.

defined zone trending through the central part of the outcrop (Figure 8). Faults of System 1 typically are short (2-5 m) and have irregular traces, suggesting that movement is dip-slip dominant. These faults have gouge thicknesses on the order of 1-2 mm, indicating small displacements. System 1 faults apparently do not have a strong influence on the structural development of the outcrop.

System 2. System 2 faults consistently cut faults of System 1. Faults of System 2 strike WNW and form a well developed zone in the southwest part of the outcrop. The 10-15 m wide zone is composed of a set of steep (60° - 80°) and a set of moderate (30° - 50°), SW dipping faults. Similarly oriented faults are located in the northeast part of the outcrop (Figure 8). Spacing of System 2 faults is on the order of 0.5 m or less and locally can be very uniform. Individual faults of the system have lengths of 5-8 m, but often link up with other members to form longer traces. These faults exhibit both normal and reverse dip-slip separations of about 2-10 mm. In many cases, apparent offsets indicate that System 2 faults have a measurable component of strike-slip. System 2 faults are similar in nature to faults that compose other WNW trending fault zones observed elsewhere in the surrounding study area.

System 3. In the south-central part of the outcrop, faults of System 2 and System 3 overlap and mutually transect each other, indicating synchronous formation. System 3 faults are localized in a curved zone that diverges from the fault zone of System 2 at the southern edge of the outcrop changing to a N35W trend, and ultimately

Figure 8. Distribution of members of System 1 and System 2 faults in the Llano River outcrop.

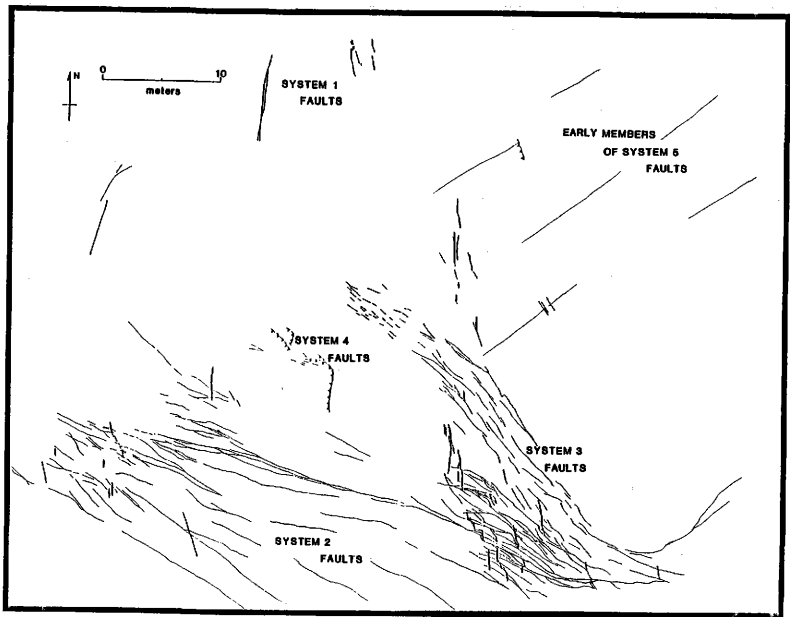


swings more westerly near its termination in the central part of the map (Figure 9). In contrast to the zone of System 2 faults, System 3 faults do not extend out of the mapped area. Near the southeast corner of the outcrop, faults of System 3 curve and merge into a N55E trending right-lateral, oblique-slip fault (Figure 9). Faults of System 3 dip from $\sim 15^\circ$ - 90° toward the SW. High and low angle faults occur in the southern part of the outcrop. In the central part of the map, the System 3 faults are shorter and have steeper dips. Displacements are dip dominant, oblique-slip (both normal and reverse) with apparent separations of 0.1 to 2 cm. A few fault surface striations, trending NE-SW with shallow to moderate plunge, were observed where Systems 2 and 3 overlap.

Other fault zones observed in the field area do not have the curved geometry that is characteristic of the zone of System 3 faults. The development of System 3 faults may be controlled locally by displacements on other fault systems in the outcrop.

System 4. Several NW-trending, low angle faults are developed in close association with cross-bed set boundaries (Figure 10). The timing of System 4 faults with respect to Systems 1, 2 and 3 can not be established due to the lack of crosscutting relationships. They are however, cut by faults of System 5. Many of the faults are small thrusts (displacements less than 1 cm) that locally follow cross-bedding. Other System 4 faults are "detachment" surfaces between major bed-sets. The thrusts and "detachment" faults are usually spatially associated but have a sparse occurrence in the outcrop. The

Figure 9. Distribution of fault system 1, 2, 3 and 4 and early-formed elements of System 5 faults in the Llano River outcrop.



detachment surface at
bedset boundary →



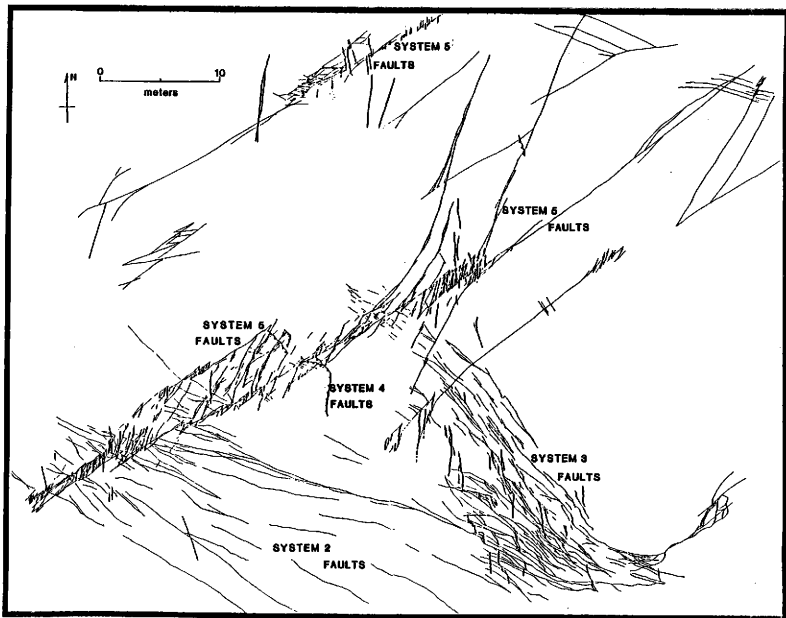
Figure 10. Detachment and thrust faults of System 4. Ruler is 15 cm long.

presence of System 4 faults indicates that local σ_1 oriented subhorizontally, resulted in decoupling between bed sets during the deformation of the sandstones.

System 5. The last system of faults to develop in the outcrop is composed of two associated sets of faults. One set is arranged en echelon and strikes N50-60E and the other set trends N to NNE and is spatially restricted to the overlap region between members of the NE trending set (Figure 11). As illustrated in Figure 9, some members of the NE trending set are interpreted to be contemporaneous with formation of Systems 3 and 4, however, none of the System 5 faults are offset by any of the older fault systems. Both sets of faults have dips ranging from 65° to 90°. The NE trending faults dip predominantly to the SE, whereas the N to NNE trending faults generally dip to the ESE. System 5 faults have highly variable lengths, ranging from centimeters up to greater than 39 m. Lengths of the members of the N to NNE trending set are controlled by the spacing between the NE trending faults that bound them.

All System 5 faults are oblique-slip, with the strike-slip component usually much greater than the dip-slip component. The NE trending faults have left-lateral separations and the N to NNE faults have right-lateral separations. In only a few cases were actual slip vectors obtainable. Displacements on the N to NNE trending faults are less than on faults of the NE trending set. The largest apparent offsets on System 5 faults are greater than on any other faults in the

Figure 11. Distribution of faults in the Llano River outcrop.

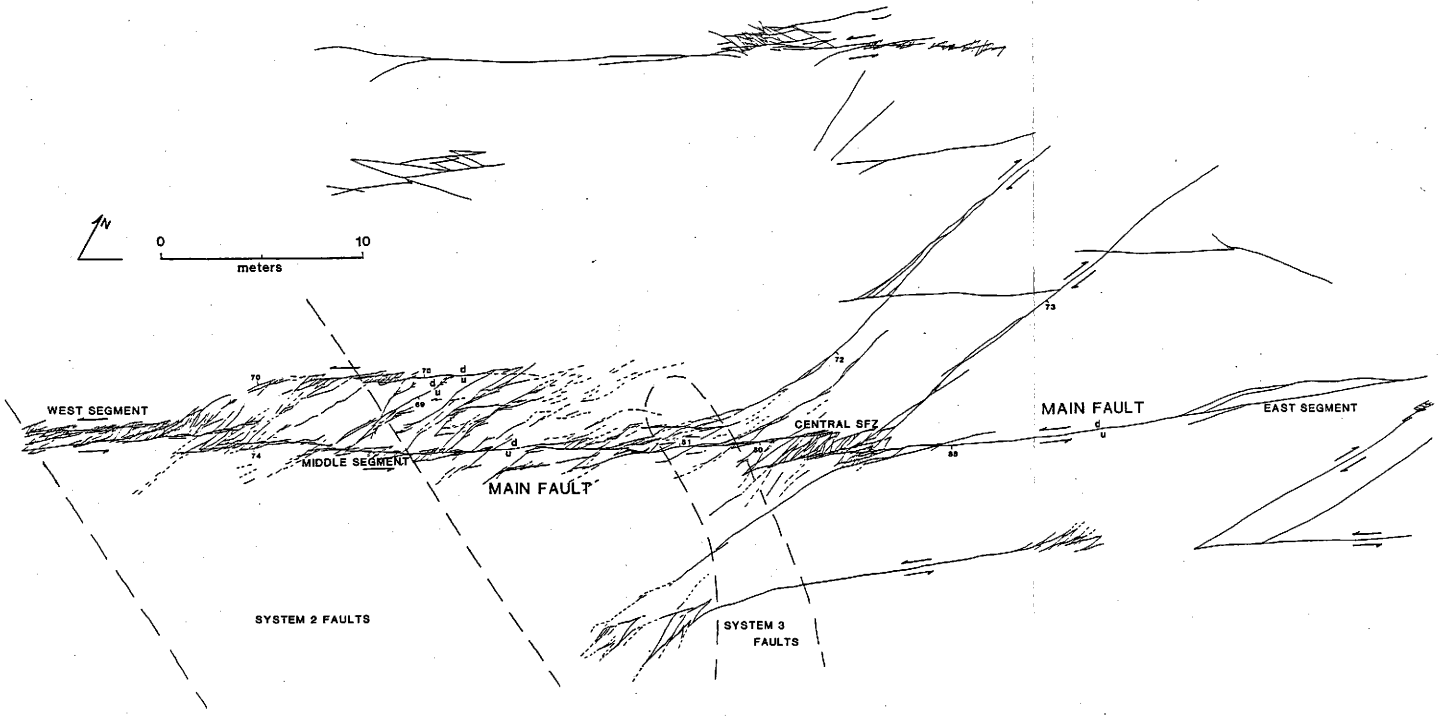


outcrop. Strike separations range from a few millimeters up to 25-35 cm. The largest dip separations are on the order of 2-4 cm.

Field relations indicate that deformation associated with System 5 initially was distributed on widely spaced NE trending fault segments (Figure 9). Therefore, System 5 is divided into a system of early formed (i.e., primary) faults and a system of associated secondary faults. The secondary faults are restricted between overlapping primary fault pairs and are either: (1) synthetic to the primary faults (i.e., oriented subparallel, with the same sense of shear as the primary faults), or (2) antithetic to the primary faults (i.e., oriented oblique to and with a sense of shear opposite that of the primary faults). This terminology follows that of Wilcox et al. (1973) for secondary faults associated with wrench fault systems. In general, the primary and secondary synthetic faults correspond to the NE trending set of faults and the secondary antithetic faults correspond to the N to NNE set (Figure 12). Fractures, represented by the dashed lines in Figure 12, occur in direct association with the primary and secondary faults. These fractures are contemporaneous with the faulting and are considered as a subset of System 5.

Main Fault. The largest offsets observed in the outcrop occur on a group of closely spaced, System 5 faults that trend through the central part of the map. These faults define the trace of the Main Fault (Figure 12). Within the outcrop the Main Fault is composed of three major segments: the West, Middle and East segments (Figure 12). These three NE trending segments are in a right-stepping en echelon

Figure 12. Map of System 5 faults showing the Main Fault and location of fault System 2 and System 3.



MAP OF SYSTEM 5 FAULTS

configuration and are linked by associated secondary faults. Where other NE trending primary faults of System 5 exhibit maximum separations of 6-10 cm, separations on the major segments of the main fault are as large as 25-35 cm. If mapped at a smaller scale, the Main Fault would probably be represented as a single, small fault.

The characteristics of the distinctive fault-zone geometry, formed by the en echelon primary faults and the associated secondary faults are the main focus of the following chapter. In order to facilitate discussion of particular aspects of System 5 faults, a given system of linking, secondary faults and the associated pair of primary faults will be referred to as a Secondary-Fault Zone (SFZ).

Fault System Relationships

The following observations indicate that many of the characteristics of System 5 faults are strongly influenced by the location and nature of System 2 and System 3 faults. Because the largest displacements in the outcrop are associated with the last stage of faulting, these relationships provide key insights into the structural development of the outcrop.

1) The West and Middle segments of the Main Fault are themselves composed of numerous short segments. Several small SFZ are developed along this part of the Main Fault. In contrast, the East segment of the Main Fault is essentially a single, continuous fault (Figure 12).

2) The change in the trace of the Main Fault, from a segmented to a continuous nature, occurs where the System 3 fault zone is cut by the Main Fault (Figure 12).

3) To the northeast of the Central SFZ, there are no well defined fault zones that are cut by System 5 faults. Only in the extreme NE corner of the outcrop does the relatively continuous East segment cut any pre-existing faults (Figure 12).

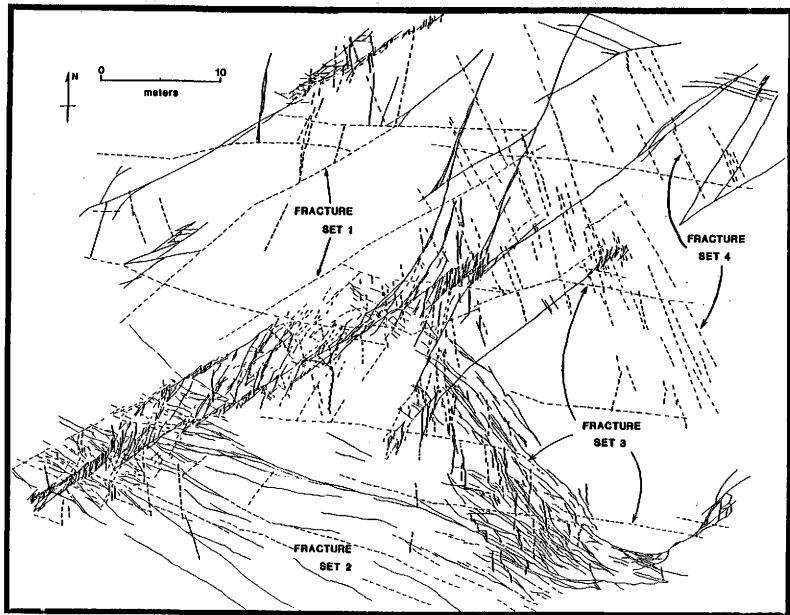
4) The right step between the West and Middle segments of the Main Fault is coincident with the area where the zone of System 2 faults is cut by System 5 faults (Figure 12).

5) The shorter NE trending primary faults that constitute the Middle and West segments have somewhat more northerly strikes (N40-55E) than the general trend of the Main Fault. There is also a prominent strike change across the Central SFZ, from N57-61E on the Middle fault segment to N50-55E on the East segment (Figure 12).

Fracture Sets

Fractures in the outcrop trend generally WNW, NNW and NE. Granite outcrops located north, south and east of the area mapped in detail also exhibit these general trends (Figure 5). Based on their orientation and distribution in the outcrop, the fractures are grouped into four sets (Figure 13). None of the fractures are cut by faults, but two of these fracture sets are spatially related to earlier-formed fault systems.

Figure 13. Distribution of faults and fracture Sets 1, 2, 3 and 4 in the Llano River outcrop.



Set 1. Fracture Set 1 trends sub-parallel to the N50-60E trending faults of System 5. In one case, a fracture is located along the trace of a pre-existing fault (Figure 13). Dips on this set of fractures generally are steep, but are hard to measure due to preferential weathering along the fracture surfaces. Fracture spacing varies from about 1 to 10 m. Fractures of Set 1 have lengths on the order of 15-25 m long.

Set 2. Set 2 fractures are situated in a WNW trending zone that is coincident with the zone of System 2 faults, located in the SW part of the outcrop (Figure 13). Many of these fractures are colinear with, and link elements of fault System 2. Similar to the faults in this zone, Set 2 fractures have moderate to steep, SW dips and are spaced on the order of 0.5 to 1 m. Lengths of Set 2 fractures are variable but usually are not longer than about 10 m. The fractures have straight average traces, but on closer inspection, the surfaces appear jagged or rough.

Set 3. Set 3 fractures trend WNW but are not localized in a zone and show no spatial relation to other fractures or faults. The nearly vertical fractures are mostly continuous, consisting of joined segments that vary in strike by 5-15°. Usually, segments that strike more WNW are longer than the joining segments. Spacing between members is highly variable, ranging from 2 to 15 m (Figure 13).

Set 2 and Set 3 fractures do not intersect and, therefore, relative timing between the sets could not be established. A few Set

3 fractures abut against Set 1 fractures, indicating that some Set 3 fractures are younger than Set 1.

Set 4. Several Set 4 fractures abut against members of both Set 1 and Set 3, suggesting that Set 4 fractures are the youngest deformation features in the outcrop. In contrast with the other sets, no iron-oxide staining is observed in association with the fracture surfaces of Set 4. Fractures of Set 4 occur mainly in the NE part of the outcrop and trend between N12-20W. The fractures have consistently moderate dips (60-70°) to the NE, and have very linear traces. Lengths of Set 4 fractures are short (2-5 m). The fractures generally have close but variable spacing, ranging from 0.1-0.2 m up to 5 m (Figure 13). Groups or adjacent pairs of Set 4 fractures often have a distinct en echelon arrangement that is not characteristic of the other fracture sets. Although members of fracture Set 4 are not spatially associated with the faults of System 1 (as is the case with System 2 faults and Set 2 fractures) they do have similar NNW trends and occur throughout a large part of the outcrop.

Discussion: Kinematic Model of Faulting in the Outcrop

Field relations obtained from field and outcrop mapping provide the basis for a kinematic model of faulting in the outcrop. Prior to presenting the interpretation, several important points should be reiterated: 1) there are numerous, spatially varying, fracture trends in the basement, many of which probably have a Precambrian origin, 2) small-fault trends in the sandstone correlate to fracture trends in

adjacent basement outcrops, 3) fault systems in the outcrop follow a definite sequence of formation, 4) the development of the last fault system appears to be influenced by the nature and location of earlier fault systems, and 5) fractures post-date faults and the diverse fracture trends in this outcrop correspond to fracture trends in adjacent basement outcrops, and some fractures are spatially associated with faults in the sandstone.

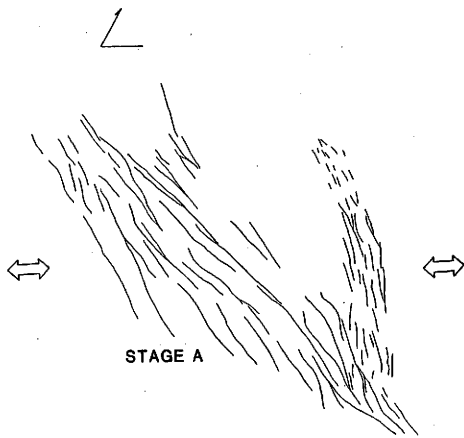
The premise of the model is that reactivation of pre-existing surfaces of weakness in the basement, controls development of faults in the overlying sandstone. Also the mechanical nature of porous sandstone is such that very small shear displacements (0.5 mm and less) will generate clearly discernable, macroscopic faults. Thus sandstone, which directly overlies the basement, can act as a tape recorder, reflecting even small movements along basement fractures. The validity of this analogy depends, in part, on the continuity of displacement or coupling across the basement/sandstone interface. In a situation where the renewed motion on a pre-existing fracture is dip-slip only, continuity of displacement into the sandstone would require that the fault in the sandstone have a very similar strike but not necessarily the same dip as the basement fault (cf. Patton, 1984). In the other end member case, where a fracture is reactivated in a strike-slip sense, potential decoupling or discontinuous deformation across the basement/sediment interface, could result in faults in the sandstone oriented at some systematic angle to the basement fault (cf. Bartlett, 1980; and Wilcox et al., 1973).

System 1 faults have very small offsets and are not strongly developed in the outcrop. There is no indication that faults of System 1 have a significant influence on the formation of later fault systems.

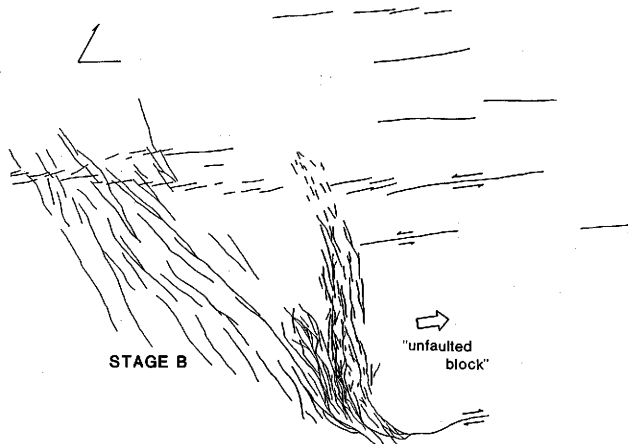
Faults of System 2 and System 3 have oblique slip with significant components of dip-slip. These two fault systems are interpreted to be generated by movement along similarly oriented fracture/fault zones in the basement. The basement fracture/fault zone associated with System 3 faults would have limited dimensions and may be only locally developed. In contrast, the System 2 faults are continuous to the WNW and have characteristics similar to other WNW trending fault zones observed in the study area. For example, System 2 faults in the NE edge of the outcrop may be members of a partly exposed fault zone (Figure 8). The proposed basement fault zones associated with System 2 faults may be part of a more extensive fracture system that was reactivated during the early stages of deformation. There are well defined fracture zones oriented WNW in granite outcrops on the south side of the river (Figure 9, rose G₁). The normal and reverse, oblique movements on faults of these two systems are inferred to accommodate lateral displacements in a NE-SW direction (Figure 14, Stage A). The total amount of extension or compression associated with the faults is unknown, as indicated by the double pointed arrows.

As deformation proceeded, the curved faults of System 3 formed in association with concurrent motion on an early-formed, right-lateral

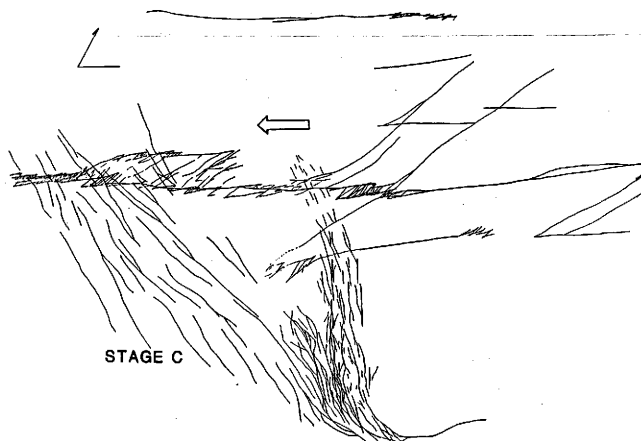
Figure 14. Kinematic model of fault development in the Llano River outcrop.



STAGE A



STAGE B



STAGE C

fault of System 5 (Figure 14, Stage B). This occurred contemporaneously with formation of other early members of System 5. Relative translation of the "unfaulted block" of sandstone toward the NE, as indicated by the arrow, is inferred by the sense of shear on the faults that bound the block, possibly reflecting translation of a discrete basement block (Figure 14, Stage B). This lateral translation could also be contemporaneous with the formation of the low angle faults of System 4. The trend of these thrust and "detachment" faults is approximately perpendicular to the inferred direction of lateral translation (Figure 14, Stage B). The lateral movements along the low angle faults of System 3 and System 4 in the sandstone, do not require continuity of deformation across the sediment/basement interface.

The influence of System 2 and System 3 faults on the development of System 5 faults is manifest by variations in length of the NE trending members of System 5. In general, the NE trending members in the SW half of the outcrop are shorter than those in the NE half (Figure 14, Stage B). The short members cut the basement-controlled System 2 and System 3 fault zones. In contrast, there are no distinct fault zones cut by the longer faults in the NE. Thus, the faults that compose the West and Middle segments of the Main Fault are initially more distributed and shorter than the East segment.

In addition, the early formed segments of the West and Middle faults of the Main Fault align in a N57-61E trend but have individual strikes ranging from N45E to N57E. The longer faults in the NE part of the outcrop strike between N50E and N55E.

If the NE trending members of System 5 correlate to a system of small faults in the basement, then the above observations suggest two interpretations:

1) the dip component of slip is great enough or occurred prior to strike slip so that the location and strikes of faults in the sandstone correspond directly to underlying basement faults. The presence of the pre-existing WNW and NW trending fault zones impeded the formation of a continuous, throughgoing Main Fault, or

2) the strike-slip motion dominates so that the distribution and strikes of faults in the sandstone are systematically arranged above a basement fault. This would be consistent with the fault that many of the early formed segments of the West and Middle faults are oriented at an angle to the Main Fault trace. There is no definitive evidence that would absolutely support one interpretation over the other.

The final stage of fault development includes the generation of the N to NNE trending secondary faults of System 5 and the formation of the Main Fault. Largest relative displacements were focused along segments of the Main Fault (large arrow, Figure 14, Stage C). Given the proximity of the outcrop surface to the basement/sediment interface, the pattern and distribution of faults in the basement may be similar to that observed in the outcrop. There is no evidence to indicate that any further motion occurred on any of the System 1, 2, 3 or 4 faults. The dominance of NE trending faults late in the deformation history of the outcrop may indicate that the regional NE trending

fault fabric was generated after initial adjustments along pre-existing faults and fractures in the basement.

The distribution and orientation of post-faulting fracture sets is also influenced by basement discontinuities. Fracturing in the sandstone late in the structural development of the area may be related to the response of the basement to stress release during erosion.

CHAPTER III

CHARACTERISTICS OF SECONDARY FAULT ZONES
BETWEEN EN ECHELON, INTERACTING OBLIQUE SLIP FAULTS

A Secondary-Fault Zone (SFZ) is defined here as a system of faults that localize between and form in response to interaction between primary faults. The initial geometry of a SFZ is controlled by the configuration of the bounding pair of primary faults. This study focuses on the specific case where the bounding primary faults overlap and step opposite to their sense of shear (when viewed parallel to the fault plane and perpendicular to the direction of movement, Figure 15). The term primary fault is used to refer to those elements of the SFZ that are interpreted to be first or earliest formed. Secondary faults are interpreted to form in response to stresses derived from interaction between the primary faults. The secondary faults exhibit systematic spatial relationships to themselves and to the bounding primary faults. Thus, faults that compose a SFZ are arranged in a distinctive pattern or fault zone geometry.

The first objective of this chapter is to establish a clear physical picture of the geometry of SFZ observed in the outcrop. This includes specification of the kinematics of the faults that compose the SFZ. These characteristics are illustrated with diagrams of an Elementary SFZ and a more complicated Compound SFZ. Examples of SFZ proceed from simple to complex.

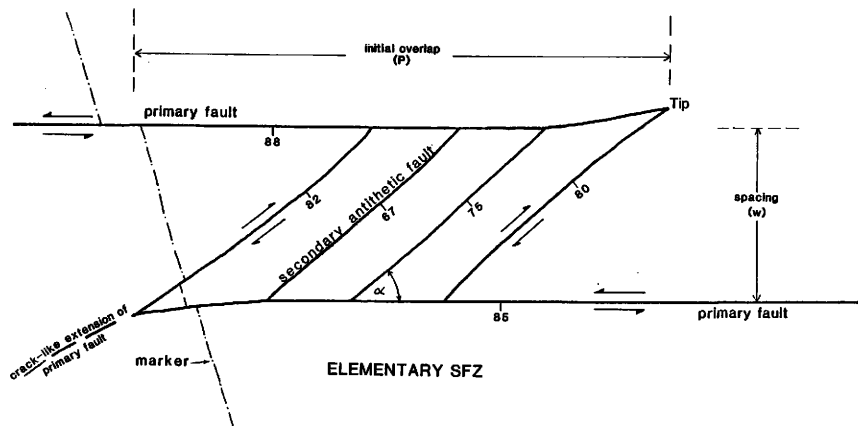


Figure 15. Schematic illustration of an Elementary Secondary-Fault Zone.

Secondly, the characteristics of the secondary faults and their relationships to bounding, primary faults are presented. This includes observations on the nature of intersections between secondary faults. From these relationships, a scenario of the development of a well documented SFZ is formulated. These and additional observations on the nature of displacements within SFZ provide the basis for the interpretation that continued displacement on the bounding primary faults is transferred, across the overlap region, through the system of secondary faults.

Geometry of Secondary-Fault Zones

An important attribute of SFZ is that they exhibit a high degree of geometric similarity at a range of scales. This can be illustrated by a cursory, visual inspection of the map of System 5 faults (Figure 15). Analysis of the length versus width dimensions of several SFZ are presented in a following section. Through extensive investigation of numerous SFZ in the study area, it is possible to synthesize an Elementary SFZ (Figure 15).

The Elementary SFZ represents the simplest possible SFZ geometry. In the schematic illustration of Figure 15, steeply dipping, bounding, primary faults have left-lateral slip and are in a right-stepping configuration. Restricted to the overlap region is a first-order system of right-lateral, secondary antithetic faults that terminate against the primary faults. The angle between a primary fault and an associated secondary antithetic fault, measured counterclockwise, is

acute.* Within a given SFZ, secondary antithetic faults generally have uniform dip directions with dips ranging from 60° to near vertical. The secondary faults, in this most simple case, are inferred to have formed synchronously.

An important aspect of the Elementary geometry is that, outer antithetic faults occur at the end of an associated primary fault. The mutual termination of the two faults forms a discrete "Tip". It is not uncommon for the trend of a primary fault, near the Tip, to change so that the fault curves away from the overlap region of the bounding faults (Figure 15).

Occasionally, the trace of a primary fault may continue beyond the Tip. However, the end of the primary fault, as marked by the absence of a continuous gouge zone, occurs at or near the tip. The trace of the bounding fault beyond the Tip, cartooned as a dashed line, is more fracture-like (Figure 15). Generally, gouge is absent or only locally developed. Shear displacements beyond the Tip, if observed, are small (~ 2 mm or less).

The essence of the Elementary geometry is observed in all of the SFZ in the study area and is a fundamental characteristic of SFZ. In general, however, SFZ observed in the sandstone outcrops have more than one system of secondary faults, and are referred to as Compound

*Similarly, a mirror image of Figure 28 would illustrate a SFZ formed between left-stepping, right-lateral primary faults. The angle, measured clockwise, between a primary and a secondary antithetic fault is acute.

SFZ. Within Compound SFZ, the Elementary geometry occurs as second (and higher) order subsystems of secondary faults (Figure 16). In addition to obliquely-oriented secondary antithetic** faults, compound SFZ have secondary synthetic** faults that are subparallel to, and have the same sense of shear as the bounding primary faults. As illustrated by the diagram in Figure 16, synthetic faults usually cut earlier formed antithetic faults and are located between the overlapping primary faults. Also, a given synthetic fault is more directly associated with, and forms adjacent to one or the other primary faults (i.e., they do not form midway between the bounding primary faults).

Subsystems of antithetic faults form between a synthetic fault and the neighboring primary fault (or between two synthetic faults). Subsystems occur either between the synthetic and its associated (nearest) primary fault or between the synthetic and the other primary fault or both. The antithetic faults of a given subsystem are assumed to be synchronous.

Figure 17 shows an example of a Compound SFZ formed between two right-lateral, left-stepping primary faults, spaced 2-4 cm apart. A single synthetic fault offsets an earlier formed (first order) antithetic fault. In this case, the synthetic fault is connected directly to its associated primary fault. A subsystem of second-order antithetic faults is bounded by the synthetic fault and the other primary fault. The antithetic faults clearly do not extend beyond the

** Subsequent reference to an antithetic or a synthetic fault implies reference to a secondary fault.

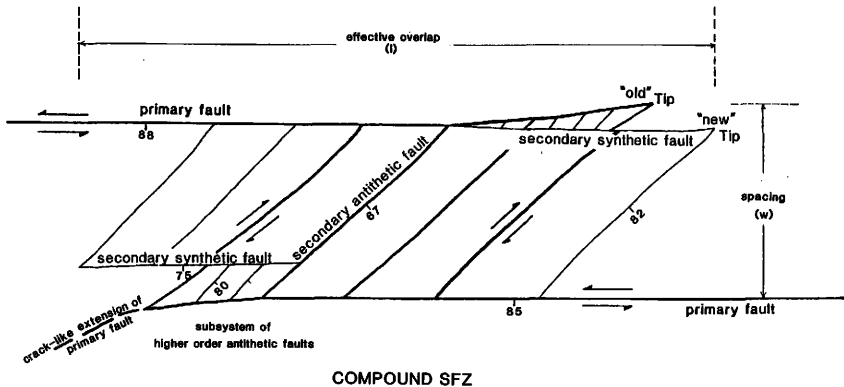


Figure 16. Schematic illustration of a Compound Secondary-Fault Zone.



synthetic fault cutting antithetic fault

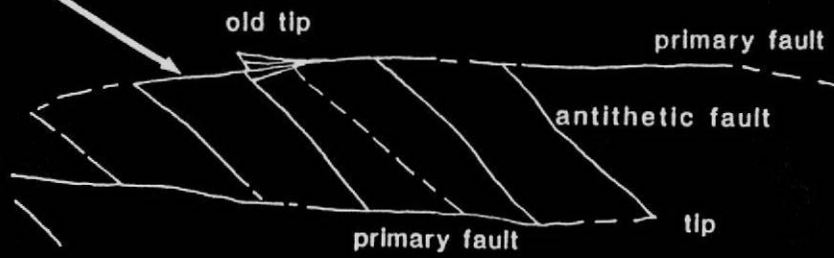


Figure 17. Example of a simple Compound SFZ. Divisions on ruler are in centimeters.

bounding faults. Cross cutting relationships establish the relative timing between the "old" and "new" tips. This SFZ is a simple Compound SFZ, having only one synthetic fault and subsystem of antithetic faults. This example closely resembles the geometry of an Elementary SFZ (Figure 15). The primary and secondary faults of this SFZ are very thin and have very small displacements (~ 2 mm and less).

Complex Compound SFZ have multiple synthetic faults and associated subsystems of antithetic faults that form adjacent to one or both of the bounding primary faults. The Central SFZ, located between the Middle and East segments of the Main Fault, is an example of a complex Compound SFZ (Figure 18). The bounding primary faults of this SFZ have apparent left-lateral offsets of 25-35 cm and displacements on the secondary faults range from millimeters up to 12-14 cm. Field observations indicate that the relative complexity of SFZ is partly a function of displacements on the faults.

There can be strong variations in morphology between individual SFZ. The sense of slip, however, on the antithetic and synthetic faults is consistent in all cases. Also the basic configuration of faults, as illustrated by Figures 15 and 16, is developed consistently over a broad range of scales.

Dimensions of Secondary-Fault Zones

Field observations indicate that length to width ratios of SFZ (Figures 15 and 16) are apparently scale independent. There are definite systematics to the positioning and sequence of formation of

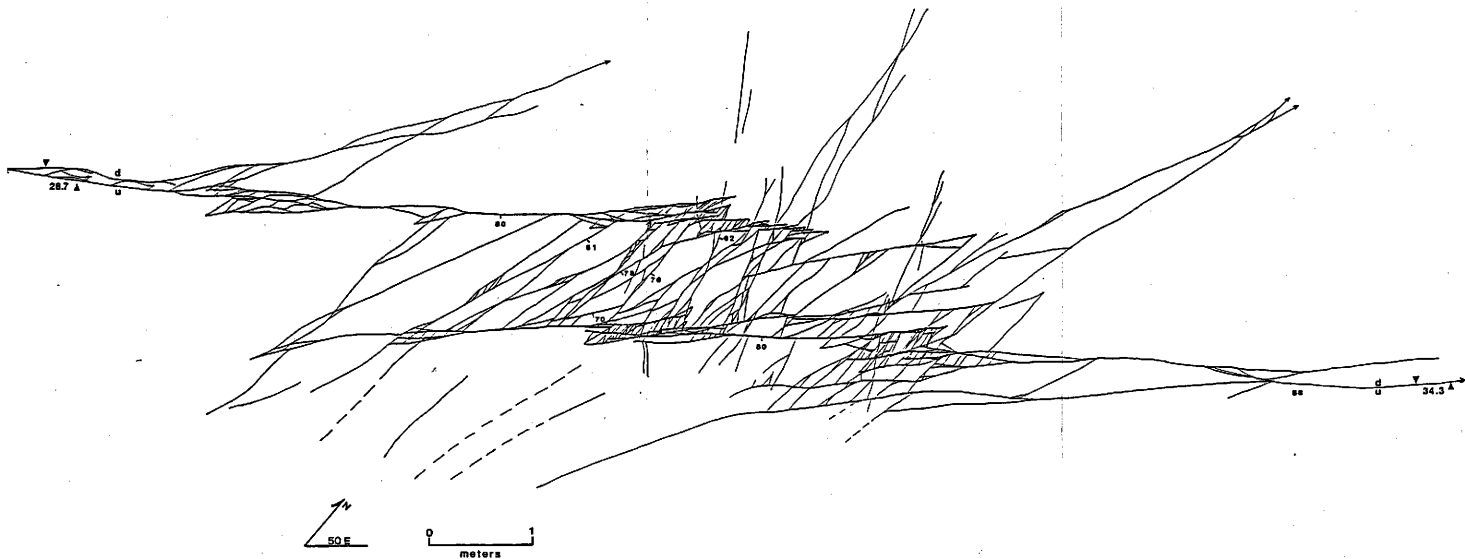


Figure 18. Map of the Central SFZ, an example of a complex Compound SFZ.

synthetic faults (to be discussed in the next section), that indicate that SFZ can lengthen with increased displacements. Thus it is possible to distinguish between the initial overlap of a pair of bounding primary faults and the effective overlap (or total length) of a SFZ (Figure 16). Observations indicate that the width of a SFZ is the same as the spacing between bounding, primary faults and does not change with development of the SFZ.

The initial overlap (P) versus width (w) of eleven SFZ are shown in a log-log plot in Figure 19. The paucity of data points reflects the difficulty in identifying the initial overlap of a pair of bounding faults in complex Compound SFZ. Ratios of P to w range from 1.85 to 4.91 and have a mean of 2.93. Linear regression of the data yields the relationship

$$P = 2.87 w^{0.97} \quad (1).$$

This result indicates that a nearly linear relation exists between initial overlap and width of SFZ (if the exponent in (1) were equal to one, the relation would be strictly linear).

A compilation of data from strike-slip fault systems throughout the world includes a log-log plot of dimensions of 70 SFZ ranging in scale from 20 to 80,000 meters long (Aydin and Nur, 1983). In this case, the data was not distinguished on the basis of initial overlap and effective overlap. Analysis of the data yields a linear relation between length and width of $\lambda \approx 3.2 w$, where λ could be either initial

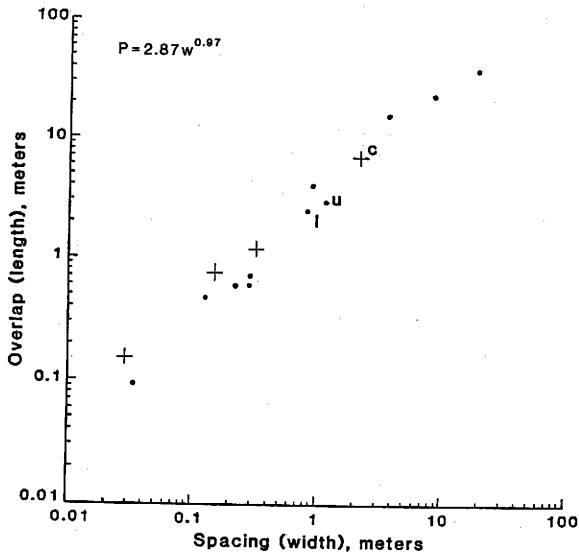


Figure 19. Log-log plot of initial overlap (P) and effective overlap (L) versus spacing (W) of primary faults from SFZ in the Llano River outcrop. Dots are data of initial overlap versus spacing; +s are data of effective overlap versus spacing. Data points l, u and c are from the lower part and upper part of the Central SFZ and from the entire Central SFZ, respectively.

overlap or effective overlap. Similar data from 20 SFZ exposed in a South African gold mine, have an average $\lambda/w = 4.1$ (McGarr et al., 1979).

With this in mind, the effective overlap (L) versus width for four SFZ from this study are also plotted in Figure 19. The four L/w values have a mean of 4.24 and the maximum L/w ratio is 5.46. A linear regression of all fifteen data points yields

$$\lambda = 3.24 w^{0.94} \quad (2),$$

where λ is initial overlap or effective overlap. Combining the data does change the relationship. The significance of the change is not known given the small data set, however, the exponent in equation (2) is less than in equation (1), suggesting that λ/w may have a scale dependent nature. Considering the relationships obtained from this study, along with the other data sets, suggests that length to width ratios of SFZ are commonly on the order of 3 to 4, and range from about 1.5 to between 5 and 6.5.

Characteristics of Secondary Faults

Antithetic Faults

Traces of antithetic faults may be relatively straight, (Figures 15 and 16), but more commonly they are curvilinear (convex or concave toward the overlap region) or sigmoidal (Figures 17 and 18). Due to

the differences in shape, a system of related antithetic faults may or may not be parallel. However, they often appear uniformly spaced in proportion to the spacing of the bounding primary faults. A few measurements, from SFZ in the area of detailed mapping, give a rough estimate of about 3:1 primary fault spacing to antithetic fault spacing. Typically only three to five antithetic faults are formed within an Elementary SFZ.

In addition to shape, the orientation of antithetic faults with respect to their bounding faults is highly variable. A frequency plot of 161 measurements of α (the acute angle between an antithetic fault and its bounding fault) shows that α ranges from 12° to 62° (Figure 20). Most of the data plots between 22° to 47° (mean = 36.7°). Within any given SFZ, α varies only 10 - 15° . Also, because of the shape of an antithetic fault or due to non-parallel bounding faults, α is not necessarily the same at both ends of a given antithetic fault. In some cases α is smaller at Tips, however, α does not appear to vary systematically with position along the bounding fault.

Visual inspection of numerous SFZ indicates that α may increase as the spacing between bounding faults decreases. For example the subsystem of antithetic faults, within the outlined area B in Figure 18, form consistently higher angles ($\alpha = 47^\circ$ to 62°) with the primary faults than in other parts of the zone. It is, however, not always possible to definitively associate a specific antithetic fault to its bounding fault pair because of the numerous fault intersections within

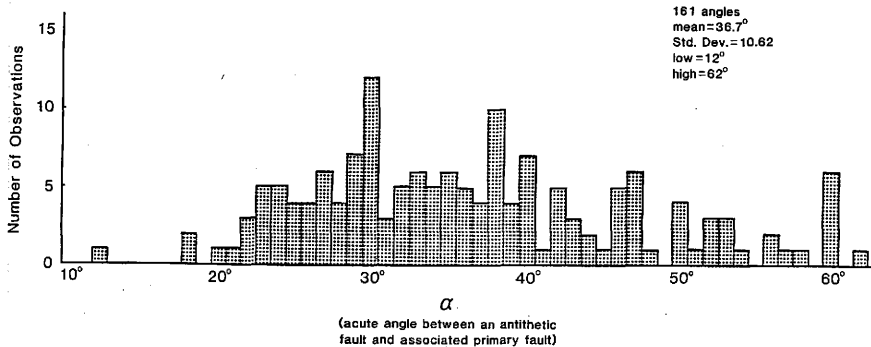


Figure 20. Frequency plot of values of α .

complex Compound SFZ. Thus, the apparent systematic change of α with spacing between bounding faults was not confirmed in this study.

Synthetic Faults

In contrast to antithetic faults, synthetic faults have straight to slightly undulating traces. Similar to primary faults, they may curve away from the region of overlap, and they form tips with outer antithetic faults. As stated previously, synthetic faults always form between a pair of primary faults.

Spatially, there are two basic relations between a synthetic fault and its associated primary fault. In one case, the synthetic fault is connected directly to the primary fault. This type of synthetic fault/primary fault association is seen in Figure 17 and illustrated as a Type 1 synthetic in Figure 21. A second case (Type 2 Synthetic) is characterized by not being connected directly to the primary fault. Type 2 synthetic faults abut against older or contemporaneous antithetic faults (Figure 21). Several examples of both types of synthetic faults can be seen in Figure 22, which is a more detailed map of part of the Central SFZ (Figure 18).

The synthetic faults in the map of Figure 22 form a group of right-stepping, apparent left-lateral offset faults that are associated with the bounding primary fault. Multiple subsystems of antithetic faults are formed between pairs of synthetic faults. The synthetic faults consistently cut earlier formed antithetic faults. These relationships indicate that younger (higher order) synthetic

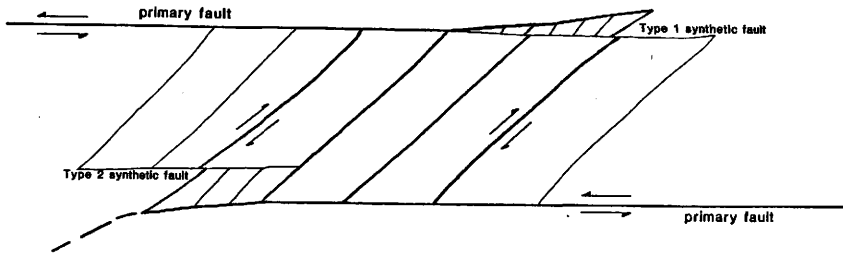
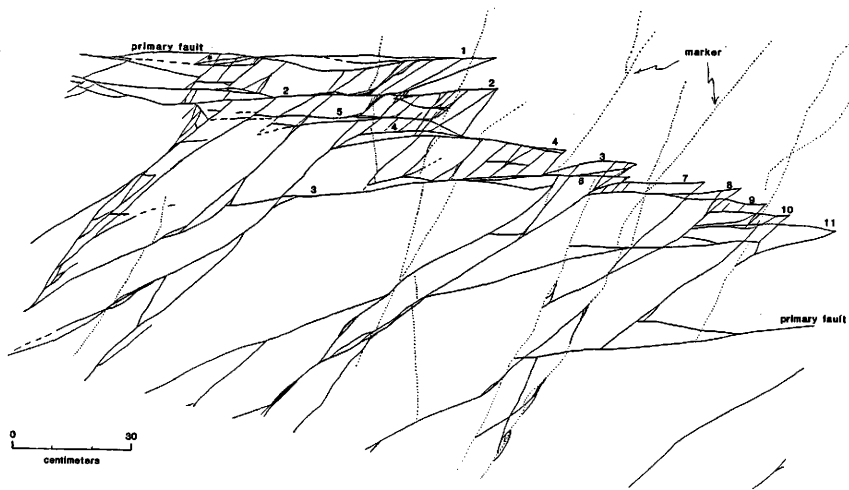


Figure 21. Types of synthetic faults.

Figure 22. Detailed map of part of the Central SFZ. The synthetic faults generally young toward the right. Both Type 1 and Type 2 synthetic faults are observed.

numbered faults
indicate age sequence



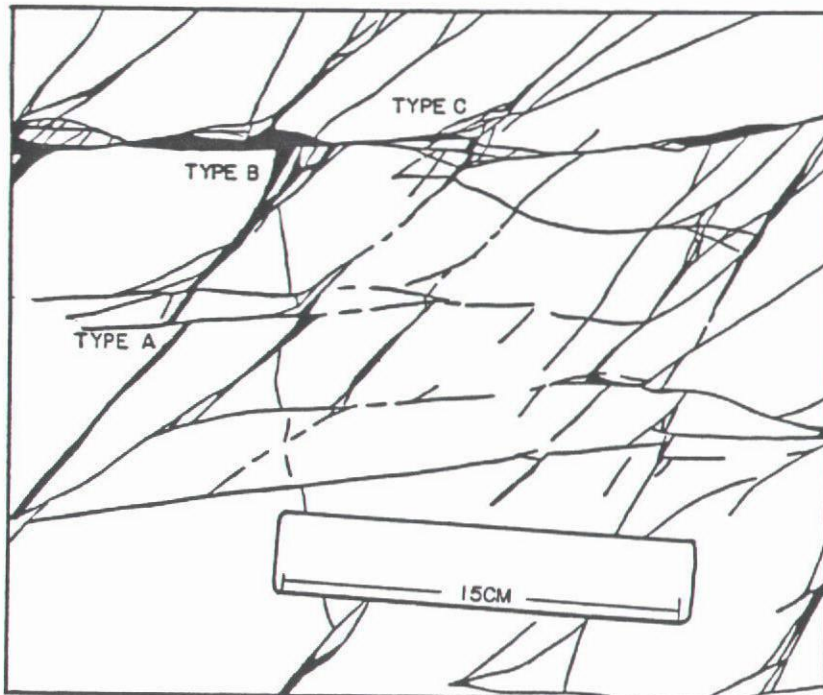


Figure 23. Types of secondary fault intersections. Details of the different types are given in the text.

faults form ahead of as well as on the interior side of older synthetic faults. For example, the right-stepping faults in Figure 22 generally young toward the right, from the primary fault to synthetic fault number 11. Generation of synthetic faults in this sequence serves two purposes. First, by propagating ahead of the primary and older synthetic faults, the overlap region of the SFZ is effectively increased. Second, by forming on the interior side of older faults, the step or spacing between interacting pairs is reduced.

Intersections Between Antithetic and Synthetic Faults

In some cases, offsets of sedimentary features or early formed faults, provide information on the sense and amount of displacement on secondary faults. More often, kinematic data is obtained from intersections between antithetic and synthetic faults. Investigation of these intersections indicate that in general, synthetic faults cut antithetic faults. However, timing relationships between secondary faults can be complex. The key to understanding the complexities is to study the nature of the secondary fault that is offset.

Three types of secondary fault intersections can be identified by comparing the nature of the faults at the intersection with the nature of the faults away from the intersection. In a Type A intersection, the offset fault has a constant trend and uniform gouge thickness (Figure 23). In a Type B intersection, either or both parts of the transected fault have a gouge zone that thickens toward the corner formed by the intersection (Figure 23). The offset fault has a

splayed or wedge geometry that abuts against the younger fault. In this case, the younger fault may show a similar change in character, near the intersection. In a Type A intersection, the nature of the younger, cutting fault is usually unchanged near the intersection. In a Type C intersection, neither fault clearly transects the other. Instead, the faults appear to "fray" into several thinner gouge zones as they approach the intersection. The synthetic and antithetic fault "strands" may cut each other, or there may be no observable offset by either fault. The intersection has an intertwining or knotted appearance (Figure 23).

As mentioned previously, there is a relationship between fault displacement and the thickness of fault gouge in a porous sandstone. In general, greater displacements generate thicker faults. Also, if other parameters such as porosity and grain size are held constant, a given displacement should generate a fault gouge zone of fairly uniform thickness. Fault characteristics at a Type A intersection indicate that there is only one period of movement on both of the faults. The relative timing of the faults at such an intersection is unambiguous. The thickening of part of an offset fault in a Type B intersection can be inferred as evidence for continued movement along the fault into or away from the corner at the intersection. Similarly, the multiple fault strands within a Type C intersection indicate that some displacement on intersecting antithetic and synthetic faults is contemporaneous. Consequently, the relative timing at Type B or Type C intersections is ambiguous.

Evolution of a Compound Secondary-Fault Zone

The timing and spatial relationships of faults within SFZ indicate that they develop systematically. This is illustrated by an interpretation of the evolution of a representative SFZ. The Central SFZ (Figure 12) is chosen for this exercise because many of the characteristics of this zone are common to other SFZ in the study area. The Central SFZ is prominently exposed in the outcrop mapped in detail and is the best documented example of a Compound SFZ. Reconstructing the sequence of faulting using cross-cutting relationships and SFZ characteristics established a working model of SFZ development. The model provides insight into the nature of fault interaction. A generalized model is presented in the conclusion chapter.

The evolution of the Central SFZ is presented in four progressive stages of development. The first stage shows the configuration and distribution of primary faults prior to formation of associated antithetic faults. The final stage shows the SFZ as it presently appears in the outcrop. Intermediate stages are constrained by the nature of the field relations. No specific interval of time or displacement is implied between each stage.

The methodology used in the interpretation is to first identify the earliest formed faults in the SFZ. Then using the observation that synthetic faults generally young toward the interior of the SFZ, and that subsystems of antithetic faults form between each "new" pair of bounding faults, the picture is "rolled forward". It is not always possible to clearly identify which bounding faults are associated with

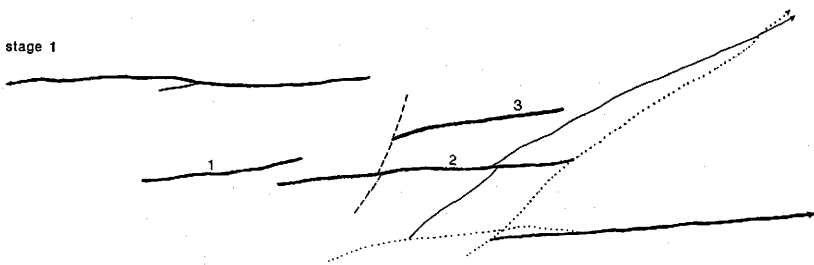
a given antithetic fault due to the nature of secondary fault intersections in complexly faulted areas (e.g., Figure 23). Where the interpretation is less well constrained, because of potentially ambiguous timing relationships, faults are shown as dotted rather than solid lines.

Stage 1. Five early formed (primary) faults are inferred from field observations: two outermost and three internal primary faults (bold lines, Figure 24). These faults have left-lateral oblique slip. The outer primary faults form a non-overlapping, right-stepping pair of bounding faults. Internal primary fault 3 is shown as terminating against a pre-existing fault (dashed), and is nearly colinear with internal primary fault 1.

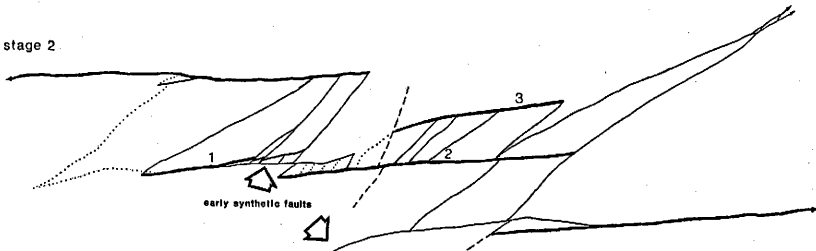
Field relations indicate that the antithetic faults (thin lines) shown in this stage, formed prior to secondary faulting associated with interaction between the five primary faults. These antithetic faults link the lower outer primary fault to another primary fault of System 5 to the north (Figure 12).

Stage 2. The earliest antithetic faults link overlapping primary fault pairs (Figure 24). At this stage of development the Central SFZ is essentially two discrete zones: an upper zone, bounded by the upper outer primary fault and by internal primary faults 1 and 2 and a lower zone, bounded by internal primary faults 1 and 2 and by the lower outer primary fault. The effective overlap between internal primary faults 1 and 2 is increased by the early development of a synthetic fault. Subsystems of antithetic faults, associated with the

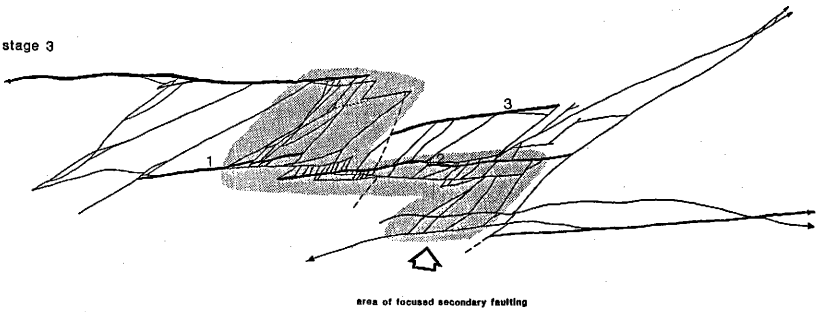
stage 1



stage 2



stage 3



stage 4

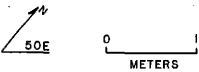
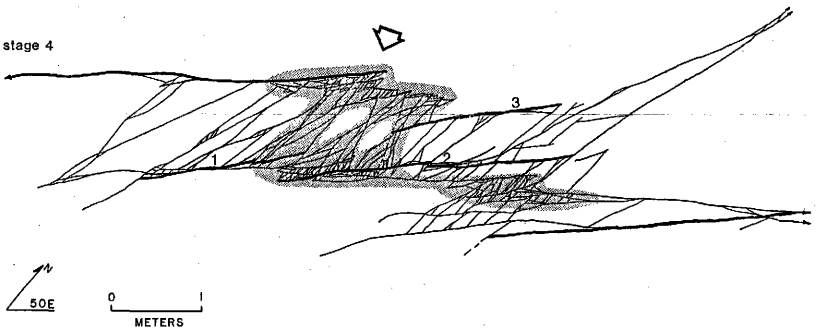


Figure 24. Evolution of the Central SFZ.

synthetic fault, link the closely spaced internal primary faults 1 and 2, effectively forming a single fault. The overlap region of the lower zone is also increased by the presence of an early formed synthetic fault. The upper outer primary fault and internal primary fault 3 do not overlap and are not linked by secondary faults.

Stage 3. With continuing development, additional synthetic and associated subsystems of antithetic faults form. The majority of "new" secondary faults are localized in an "S" shaped area (stippled region, Figure 24). As stated previously, synthetic faults adjacent to the upper outer primary fault form toward the interior and extend the overlap region of the upper zone (Figure 22). Synthetic faults in the lower zone consistently young toward the interior of the zone, but, in contrast, the overlap is not increased beyond that in Stage 2.

Stage 4. The general appearance of the Central SFZ in the final stage of development is similar to Stage 3. Additional secondary faulting is concentrated toward the middle part of the zone. The total length of the SFZ does not increase. Because no synthetic faults formed outside the outermost primary faults, the width of the zone is constant throughout the evolution. The spatial distribution of the majority of new secondary faults is more restricted than in Stage 3 and displacements are focused on fewer faults. Synthetic faults in the upper zone have effectively lengthened the upper outer primary fault, achieving overlap with the internal primary fault 3. Later forming synthetic faults in both the upper and lower zones are

of Type 2 (Figure 21) and appear to tie into the outer primary faults away from the Tip regions.

This scenario of SFZ evolution emphasizes the importance of overlap of bounding-faults prior to becoming a directly linked, interacting pair. The outer primary faults of the Central SFZ do not overlap and are not directly linked. Instead, the Central SFZ developed as a composite zone. The upper and lower zones are discrete but related parts of the Central SFZ. The internal primary faults 1 and 2, allow indirect interaction between the outer primary faults.

As suggested by the inferred development of the lower zone, if overlap is sufficient then the role of synthetic faults is only to reduce the spacing between interacting faults. In other cases, synthetic faults young ahead of one another, allowing nearly-in-plane propagation of the bounding primary fault, as well as reducing the step between interacting faults. The secondary faults connect the outer bounding primary faults in a nearly diagonal zone forming a longer, effectively continuous fault.

Since the region of secondary faulting becomes narrower with increasing development, it is hypothesized that the diagonal zone eventually would be replaced by a single synthetic fault, bypassing the SFZ, directly linking the outer bounding faults. Evidence to support this hypothesis is obtained from observations at another SFZ. The SFZ shown in Figure 25 is located in an outcrop to the west of the area mapped in detail. In this example, the bounding faults are directly linked by synthetic faults. These linking synthetic faults

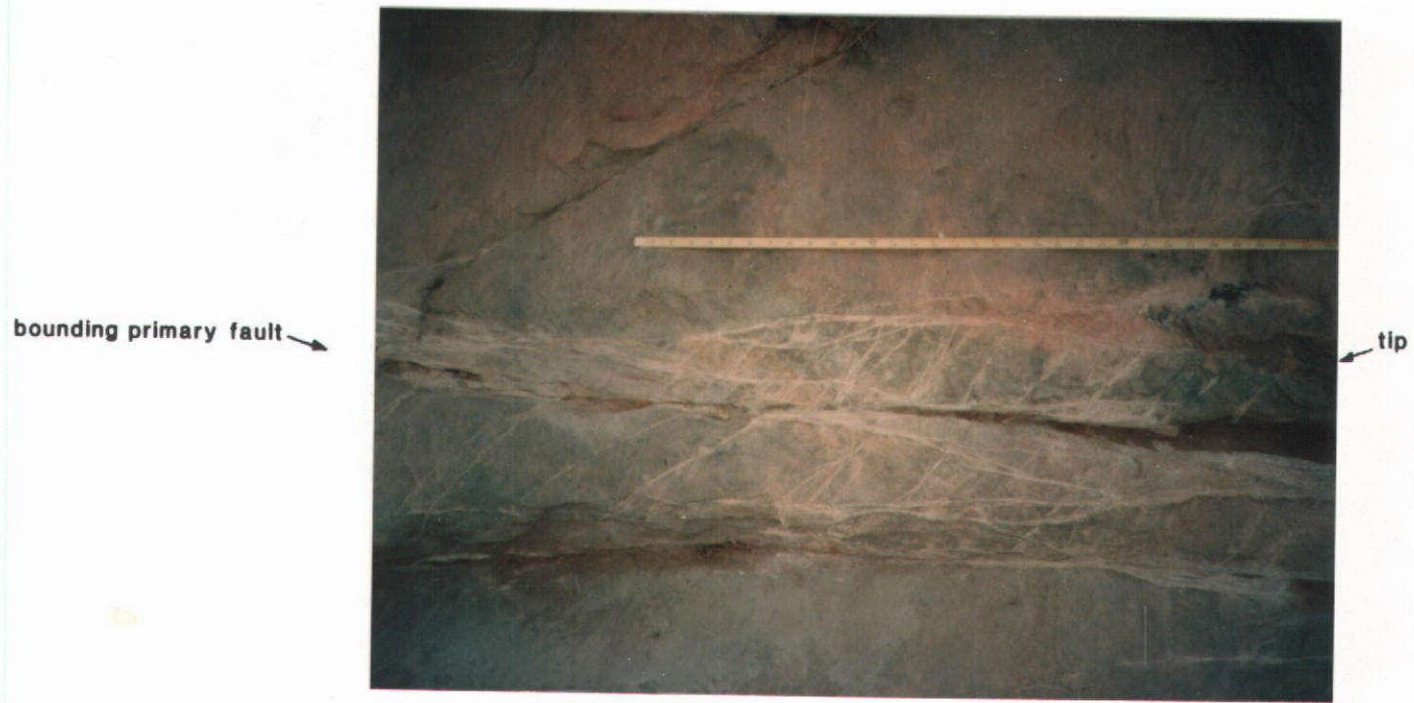


Figure 25. Example of an Advanced SFZ. Note development of synthetic faults that cut across the zone and directly link the bounding faults.

cut earlier antithetic faults and tie into the outer bounding faults in the same manner as the later formed synthetic faults in the Central SFZ. Thus, it appears that secondary faulting ultimately short circuits the step between the bounding faults into a "ramp", as the geometry evolves from a Compound SFZ to an Advanced SFZ. This scenario suggests that with increasing development displacements are not distributed throughout the SFZ but are concentrated along the most efficient path between the outer bounding faults.

Displacements

Data on the sense and magnitude of dip separations on faults in the outcrop are limited due to the nature of both the outcrop surface and internal markers. Unambiguous dip separations are known for only a few antithetic faults. In these cases the antithetic faults have normal dip separations. In contrast, bounding faults have either normal or reverse dip-slip. The following data deals primarily with strike-slip separations.

Observations indicate that displacement along bounding faults, in the overlap region, is not uniform. For example, Figure 26 is a detailed map of an antithetic fault abutting against a primary fault. Both of these faults cut elements of an earlier-formed fault system. To the right of the antithetic/primary fault intersection, the primary fault has approximately 4.28 cm of left-lateral separation. The

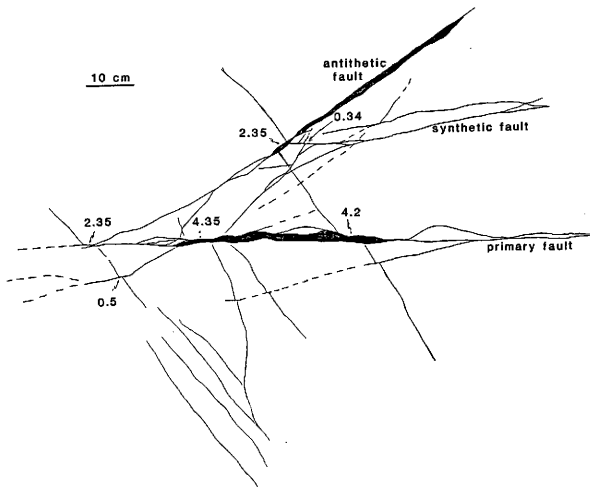


Figure 26. Detail of marker faults offset near an antithetic/primary fault intersection. All but 6 mm of the left-lateral offset on the primary fault is accounted for by right-lateral separations in the antithetic fault.

apparent offset on the primary fault abruptly decreases to 2.35 cm to the left of the primary/antithetic fault intersection. All but 6 mm of the apparent offset, "lost" by the primary fault, is accounted for by 2.35 cm right-lateral separation on the antithetic fault. This illustrates that the change in displacement on a bounding fault is directly related to the the presence of an associated antithetic fault.

As mentioned previously, outer most antithetic faults are commonly associated with terminations of bounding faults forming discrete Tips (Figure 15). In these situations, it is inferred that displacement on bounding faults need not gradually diminish to zero as required at terminations of isolated faults. A displacement discontinuity at the end of the primary fault would be accommodated by the presence of the associated antithetic fault at the Tip.

Displacement along antithetic faults appears to be uniform. This is indicated by antithetic faults that offset two or more markers. Commonly, the offsets are nearly the same and do not vary systematically with position along the antithetic fault. In addition, offset markers indicate that displacements at ends of antithetic faults is finite (Figure 24).

The inference that bounding faults and antithetic faults have finite displacements at their ends also is indicated by the fault length versus displacement relationship of some secondary faults. For example, a synthetic fault in the Central SFZ (shown dipping 80° SE, Figure 18) is approximately 3.5 m long and has 12-14 cm of apparent

left-lateral displacement. This corresponds to a ratio of fault length to apparent displacement of approximately 27:1. Similarly, a 0.3 m long antithetic fault in the Central SFZ (arrow, Figure 22), has 1.65 cm of apparent right-lateral separation corresponding to a length to displacement ratio of 18:1. Other secondary faults have length to apparent displacement ratios on the order of 75:1. Also the lower bounding primary fault of the Central SFZ, exhibits approximately 34 cm of apparent left-lateral separation but is more than 30 m long (Figure 18). The corresponding fault length to displacement ratio of this primary fault is about 88:1. The disproportionately large offsets on "short" secondary faults are possible because of the kinematic and spatial relationships between bounding faults and associated antithetic faults. Primary and secondary faults are directly connected and movement on one member of the system is related to displacement on other, interconnected members of the system.

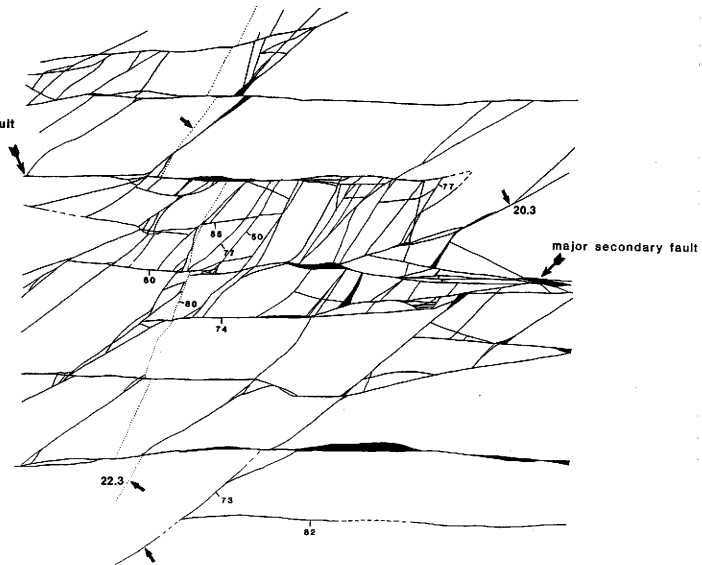
The relative amounts of displacement on a pair of interacting faults also has implications for the mechanical role of secondary faults. For example, the Central SFZ has bounding faults that exhibit nearly equal maximum displacement (Figure 18). There is approximately 29 cm of left-lateral separation on the upper outer primary fault compared to approximately 34 cm of left-lateral separation on the lower outer primary fault. In addition, two early-formed faults extend across a portion of the Central SFZ and provide information on the distribution of displacements within that part of the zone (Figure 27). The net apparent left-lateral offset of these marker faults

Figure 27. Detailed map of a portion of the lower part of the Central SFZ.

0 20
centimeters

N
50 E

major secondary fault

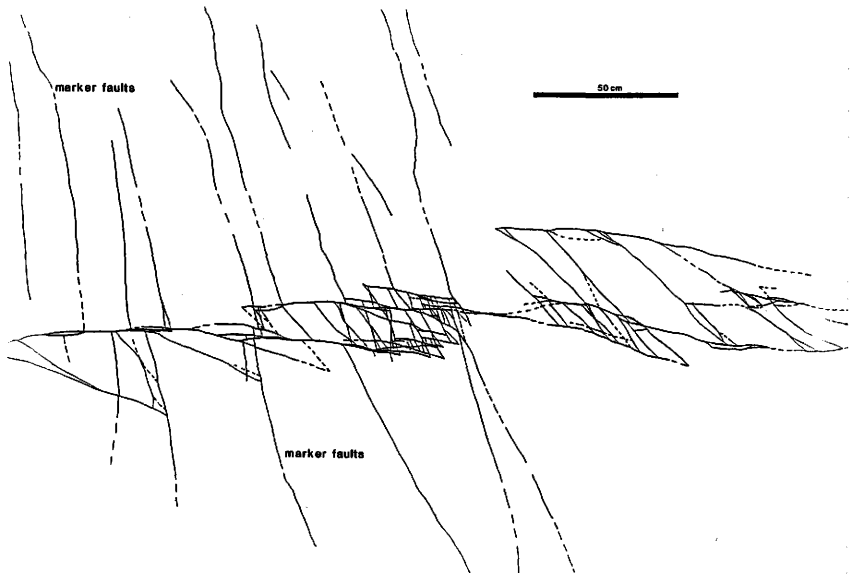


(dotted) by synthetic faults is 22.3 cm and 20.3 cm. The nearly equal offsets along these transects within the zone correspond to nearly equal offsets on the outer bounding primary faults of the Central SFZ.

A large portion of the offsets observed in the lower part of the Central SFZ, occur on two "major" synthetic faults. The major synthetic faults are linked by a complex subsystem of antithetic faults. Field relations indicate that this subsystem forms late relative to other secondary faulting in this part of the SFZ (Figure 27). This suggests that displacements are concentrated on fewer secondary faults with continued development of the zone.

Another SFZ (Figure 28) has differing amounts of displacements on the outer bounding faults. In this case the bounding faults have right-lateral strike separations and are in a left-stepping configuration. Apparent offsets of markers systematically decrease toward the right from approximately 5.5 cm to about 2.5 cm. To the right of the last marker, the faults are thinner and hard to trace (dashed faults), suggesting a continued decrease of displacement from left to right. The distribution of secondary faults within the SFZ also varies spatially. There are only a few synthetic faults developed toward the left end of the zone. Toward the right however, where apparent offsets decrease to about 2.5 cm, there are numerous synthetic and associated antithetic faults. Similar relations have been observed in other SFZ suggesting that secondary faulting may localize near one or the other of a pair of bounding primary faults when the displacement on the primary faults is not equal.

Figure 28. Detailed map of a SFZ with left-stepping, right-lateral bounding faults. Offsets of the marker faults gradually decrease toward the right.



Interpretation

The characteristics of SFZ in the study area indicate that the mechanical role of the secondary faults is to link a pair of interacting faults, allowing displacement along one primary fault to be transferred to the other bounding fault. Situations as illustrated in Figure 26 provide direct insight into the transfer process. Since displacements on antithetic faults appear to be uniform, transfer between bounding faults may be achieved in a stepwise or incremental fashion.

Situations where net offsets at different "transects" within the zone are nearly equal (Figure 27) and the displacements on the bounding faults are equal (Figure 18) indicate that all of the displacement is transferred through the secondary faults. With continued displacement and formation of directly linking synthetic faults (e.g., Figure 25), the bounding faults are effectively a continuous fault and movement on antithetic faults are no longer required in the transfer process. In other instances (e.g., Figure 28), secondary faulting, associated with one fault of an interacting pair, may provide a mechanism for displacement to be dissipated into the overlap region. Incomplete transfer of displacement through the secondary faults may also occur where the trace of bounding faults curve away from the overlap region. Beyond the Tip the character of the bounding fault commonly becomes more fracture-like (Figure 15). Some amount of strain could be dissipated into the rock near the end of the fracture.

CHAPTER IV

DISCUSSION: RELATION TO PREVIOUS WORK AND EVOLUTION
OF A TYPICAL SECONDARY-FAULT ZONE

A review of the literature reveals that features with geometries similar to SFZ observed in the Llano River outcrops are developed in all structural settings. The distinctive arrangement of faults that characterize these features is most readily identified when the plane of observation is both parallel to the slip vector and perpendicular to the bounding fault planes.

An investigation of mining-induced small faults in a quartzite, provides information on secondary faults associated with interacting normal faults observed in cross section (Gay and Ortlepp, 1979; and McGarr et al., 1979). The spatial arrangement of the secondary faults (Figure 29) is very similar to features observed in the Llano River outcrop. The zone of secondary faults does not extend beyond the overlapping primary faults and outer antithetic faults "seem to originate from" ends of primary faults (McGarr et al., 1979). Synthetic secondary faults do not occur in the middle of the overlap region but are located ahead of and adjacent to associated primary faults. Smaller systems of antithetic faults (subsystems) form between primary and synthetic fault pairs. As illustrated in Figure 29b, the primary and synthetic faults have a strong tendency to curve into the direction of far-field σ_1 (away from the zone). This character also is present in the faults in the Llano River outcrop, but is not as prominently developed.

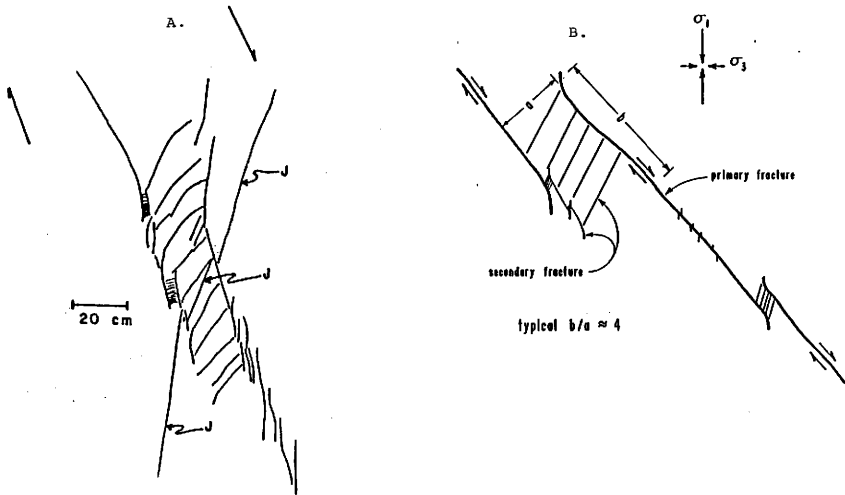


Figure 29. (A) Map of fault zone exposed in cross-section in a South African gold mine. (B) Conceptualized diagram of a typical SFZ as observed in the gold mine. From McGarr et al. (1979).

As mentioned previously McGarr et al. (1979) also report that relative dimensions of the fault systems are generally scale independent. Measurements of the overlap (b) and spacing (a) of 20 SFZ yielded ratios (b/a, Figure 29b) that vary from 1.3 to 6.6 (average: 4.1), but exhibit no systematic variation with absolute dimension. These data are in close agreement with values obtained in this study.

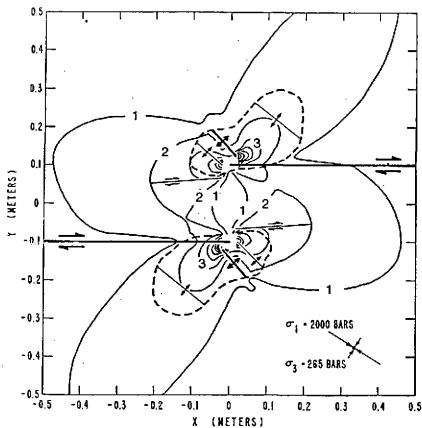
There is, however, an important difference between SFZ studied by McGarr et al. (1979) and those observed in the Llano River outcrops. In their conceptualized diagram (Figure 29b), McGarr et al. (1979) indicate that the acute angle between antithetic and bounding faults (α) is consistently on the order of about 60° . Values of α obtained in this study are as high as 62° but range as low as 12° and average about 37° . Furthermore, field observations in this study suggest that α may increase as the spacing between bounding faults decreases. This apparent systematic change of α may reflect variations in orientation of stresses within the overlap region as the distance between interacting faults becomes less. It is not clear why this relationship would be manifest in SFZ in the Llano River outcrop but not in the gold mine.

In addition to the field investigation, McGarr et al. (1979) also present a model of the faults as interacting shear cracks in a linearly elastic, isotropic material. This approach is discussed in greater detail by Segall and Pollard (1980). The two-dimensional model, which assumes plane strain, prescribes the length, spacing and frictional

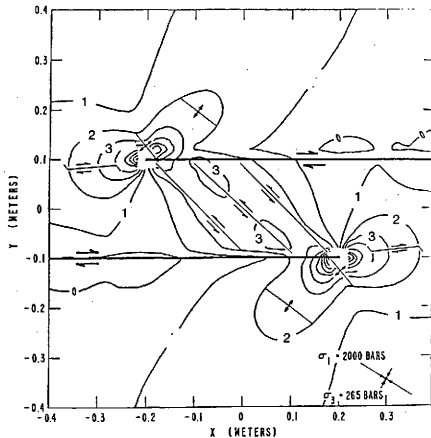
strength of the primary cracks. Subjecting the cracks to a homogeneous far field stress as indicated in Figures 30 a and b, the Mohr-Coulomb failure criteria is used to predict regions of failure and orientations of secondary shear cracks. The model is a reasonable first approximation of the strike dominant, oblique-slip fault systems observed in this study and can be used to gain insight into the mechanics of the SFZ in the Llano River outcrops.

The results from two cases, one where the primary faults do not overlap and the other where the faults have an overlap to spacing ratio of 2:1, are shown in Figures 30 a and b respectively. Solid contours in these figures are values of $F = \tau / -0.7 \sigma_n$, normalized to the far field maximum compressive stress (σ_1). Regions of high F values are areas where secondary fracturing is predicted.

For the case of no overlap between the primary cracks, lobes of high F are situated outside the step between the cracks and ahead of the crack ends. A region of induced tension (dashed contour) is similarly situated (Figure 30a). The interpretation of this analysis by McGarr et al. (1979) includes two results that are important with respect to this study. First, tensile cracks may initiate near the end of the primary cracks and propagate away from the region of interaction. This may explain the occurrence of fracture-like continuations of bounding faults beyond the Tip as observed in this study (illustrated in the Elementary and Compound SFZ geometries, Figures 15 and 16). The tendency of a bounding fault to curve away is consistent with local stress conditions as indicated in the model. Propagation



A Case of no overlap of primary cracks



B Case of overlap to spacing ratio of 2:1

Figure 30. Model of interacting shear cracks in a linearly elastic isotropic material. After McGarr et al. (1979).

of the fault into an area of low mean stress may not require formation of gouge, usually associated with small faults in porous sandstones.

Secondly, formation of the tensile crack outside the step are interpreted by McGarr et al. (1979) to releases stresses there, which could focus secondary shearing into the high-F region ahead of and between the primary cracks. The two potential failure planes, oriented at 30° to the local σ_1 have senses of shear and approximate orientations corresponding to antithetic and synthetic faults. The specific locations of the secondary shears, as noted by McGarr et al. (1979) are "somewhat arbitrary". Note, however, that for the case of no overlap an antithetic crack emanating from either of the primary cracks would not intersect the other primary crack. This supports observations in this study which indicate that some overlap is required before the bounding faults are physically linked. McGarr et al. (1979) propose that synthetic shear cracks interact with their associated primary cracks, effectively allowing the primary shears to extend nearly in plane and achieving overlap.

For the case where the primary cracks overlap, lobes of high F extend from ends of the primary cracks as in the non-overlap case. Values of high F also are generated in the overlap region promoting the formation of antithetic shear cracks between the primary cracks. As before, synthetic shear cracks are predicted to form ahead of the primary cracks. The resulting geometry of faults, as drawn by McGarr et al. (1979), closely resembles the idealized Elementary SFZ geometry (Figure 15). Thus, this mechanical analysis provides a reasonable

explanation of the attitudes and locations of the secondary faults observed in the gold mine fault system and in the Llano River outcrops. McGarr et al. (1979) point out that the predicted orientations of antithetic faults form smaller angles with the primary cracks than are observed in the gold mine fault systems. Similarly, the model does not predict the wide range of antithetic fault orientations observed in the SFZ in the Llano River outcrops.

Results from the analysis by McGarr et al. (1979) also has implications on the nature of displacement transfer. The absolute dimensions of fault length and spacing used in the model were chosen to be the same as the SFZ illustrated in Figure 29a. From the model, the net displacement across the pair of interacting primary cracks is 2.9 mm compared to an observed displacement of approximately 6 cm across the SFZ in the gold mine. However, the mechanical analysis does not allow faults to physically intersect or abut. McGarr et al. (1979) interpret the larger than predicted displacements to require inelastic deformation of the material within the overlap region. Observations from the study of SFZ in the Llano River outcrop suggests that the inelastic deformation is accommodated by transferring increments of displacement from one bounding fault to the other, effectively transforming the interacting fault pair into a single, longer fault.

A recent study by Aydin et al. (1985) analyzes the development of fault overlap using a fracture mechanics model similar to the one employed by McGarr et al. (1979). The analysis shows that interaction

between en echelon faults initially promotes and then suppresses fault propagation, achieving limited overlap. This is consistent with results from a comparison of effective overlap versus width (L/w) to initial overlap versus width (P/w) of SFZ in the Llano River outcrop. The few data points obtained suggest that L/w values are generally higher than P/w values (average ratios of 4.24 and 2.93 respectively). Also, the data from this study and from that of McGarr et al. (1979) yield maximum L/w ratios between 5 and 6.5. These observations indicate that, for a given SFZ width, there is some optimal effective overlap that allows efficient interaction between bounding faults. The secondary faulting associated with the propagation from initial overlap to effective overlap can be related to continued displacement on the primary faults. The mechanical analysis, together with the field observations support the hypothesis that in cases where continued displacement would require lengthening beyond the optimal effective overlap, the SFZ evolves from the Compound to the Advanced geometry.

Additional insight into the evolution of fault zones is provided by simple experiments which simulate deformation of sediments over a basement fault, using a layer of clay deformed in simple shear (Wilcox et al., 1973). Photographs recording the progressive deformation of the clay (Wilcox et al., 1973; Figures 7a-c and 8d-e) show that, following an initial pervasive phase of plastic strain, two conjugate sets of faults form over the "basement" fault. One set forms at a small angle to the strike of the basement fault and has the same sense

of shear. Wilcox et al. (1973) term these as synthetic faults. The synthetic faults are en echelon, and are consistently right-stepping when the sense of shear on the basement fault is left-lateral. The other set forms at an angle of about 78° to the basement fault (approximately 60° to the synthetic set) and has an opposite sense of shear relative to the basement fault. These faults are termed antithetic, and are initially restricted between elements of the synthetic set (Wilcox et al., 1973; Figure 7c). In the later stage of development with continuing displacement, a younger set of faults form subparallel to the basement fault, and transect the antithetic faults (Wilcox et al., 1973; Figure 8e). The resulting fault zone geometry resembles the configuration of System 5 faults observed in the Llano River outcrop. The strike dominant, oblique-slip faults of System 5 probably did not form under the same boundary conditions as the faults in the clay. The development of the fault zone in the clay is, however, closely analogous to the formation of the directly-linking synthetic fault in the Advanced SFZ geometry.

Additional information on the nature of secondary faulting between bounding faults is provided by detailed studies of small fault systems exposed in the Sierra Nevadas. In this case the bounding faults are strike-slip faults that nucleated along pre-existing fractures in a granodiorite (Segall and Pollard, 1983). The general geometry of these fault zones is similar to that of SFZ in the Llano River outcrops: obliquely-oriented secondary fractures are localized between the bounding faults and often exhibit small offsets opposite

to the sense of shear on the bounding faults (Segall and Pollard, 1983; Figure 10). As in the previous example, the acute angle of intersection between the antithetic and bounding faults is shown to be steeper than observed in SFZ in the Llano River outcrops. An important distinction between these fault zones and SFZ in the Llano River outcrops is that the bounding faults are essentially completely overlapping and have uniform displacements as large as ten meters or more. In this situation, with displacement concentrated at the boundary, transfer through the secondary faults is not required. The similarity of secondary fault orientations probably reflects similar stress orientations between bounding faults but the mechanical role of the secondary faults is different from secondary faults in SFZ in the Llano River outcrop.

The distinctive pattern of secondary structures also has been generated in experimentally deformed, intact rock samples (Borg and Handin, 1966). Figure 31 is a line drawing of a photomicrograph of a migmatite deformed at 1 Kbar, 150°C and a strain rate of 1% per minute. A well defined SFZ localized between the two "main" faults is evident in the center of the specimen. Borg and Handin (1966) interpret the secondary fractures to be conjugates to the main (or primary) faults. Once again, the angle between the antithetic and bounding faults (i.e., the conjugate faults) is greater than observed in this study. The ratio of overlap to spacing of the main faults is approximately 4.7 to 1. The displacement on the faults measured at the end of the sample account for about 50% of the total axial shortening. In

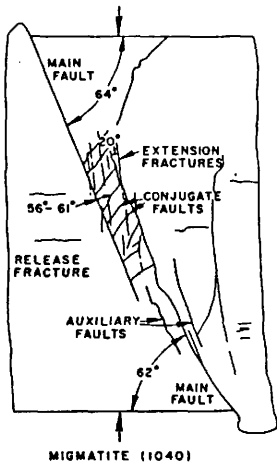


Figure 31. Line drawing of a SFZ developed in a migmatite, experimentally deformed at 1 Kbar, 150°C and strain rate of 1% per minute. From Borg and Handin (1966).

contrast to SFZ observed in the Llano River outcrops, well defined synthetic faults and subsystems of antithetic faults are not observed in the sample. Also the occurrence of extension fractures in the migmatite, oriented subparallel to the long axis of the specimen (Figure 31), was never noted in SFZ in the Llano River outcrops.

If the faults that compose System 5 in the Llano River outcrop (Figure 12) are considered irrespective of their spatial and temporal relationships, as presented in Chapter II, they can be divided into two fault sets. One set, composed of primary and secondary synthetic faults, has a N50-60E trend, and the antithetic faults make up a N to NNE trending set. Similarly, other studies (Tchalenko, 1970; Friedman and Shimamoto, 1978; Jamison, 1979; Bartlett, 1980) often "lump" elements of fault zones into sets, representing the observed fault pattern as an array of "Riedel shears". The Riedel-shear array has at least three fault sets, which usually are interpreted in terms of the Mohr-Coulomb failure criterion (Figure 32). The R_1 and R_2 shears form a conjugate pair, bisected by the maximum principal compressive stress (σ_1). The Y shear is oriented at 45° to σ_1 and parallel to the principal shearing direction. Experimental investigations of fault zone development with increasing shear displacement commonly show that R_1 and R_2 shears form early, and an additional P and the Y shears form with increasing displacement (Tchalenko, 1970). The P shears are thought to form due to kinematic constraints on the R_1 and R_2 shears, and the Y shears link the other shears to form a through going fault, parallel to the main shear direction.

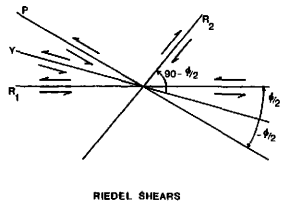
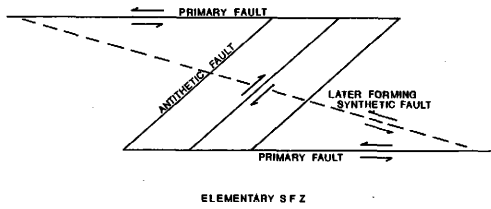


Figure 32. Comparison of the Riedel shear array to the Elementary SFZ geometry.

Neglecting the geometric characteristics of SFZ in the Llano River outcrop, primary and synthetic secondary faults could be interpreted to be analogous to R_1 shears and antithetic secondary faults would be analogous to R_2 shears (Figure 32). As discussed earlier, in the evolution from Compound to Advanced SFZ, later forming synthetic faults directly link the bounding, primary faults. This might correspond to formation of Y shears. Faults corresponding to late forming P shears have not been identified in SFZ in the study area. It is argued, however, that to indiscriminately group the primary and secondary faults into two or three elements of an array (c.f. Jamison, 1979), ignores the spatial and temporal relationships of the faults that are presented in this study. These relationships provide a greater understanding of the mechanics of the primary and secondary faults and their role in the evolution of throughgoing fault zones.

CHAPTER V

CONCLUSIONS AND MODEL OF SECONDARY-FAULT ZONE EVOLUTION

Investigation of the structural geology of the study area indicates that:

1) The study area is characterized by diversely oriented fractures and small faults that trend generally W to WNW, NW, N and NE. The relative development of these trends throughout the study area is spatially variable.

2) Small faults are the dominant structural feature in the Hickory Sandstone. The only large fault (displacement greater than 1m) identified in the study area parallels the NE trend of major normal faults in this part of the Llano Uplift. Where the sandstone is shallowly underlain by basement, trends of small faults closely correspond to fracture trends in the basement.

3) Numerous fault systems, distinguished on the basis of fault type (normal, reverse, strike or oblique-slip), orientation, distribution (location, spacing and length), and relative timing, commonly are developed within any given outcrop. For example, detailed investigation documents the existence of five fault systems developed within a single outcrop. The earliest deformation in the outcrop was associated with small dip-slip dominant offsets. Subhorizontal movements in the later stages of deformation are indicated by the presence of local detachment and thrust faults and a system of larger displacement, strike-dominant, oblique-slip faults (35 cm, maximum apparent offset). Field relations indicate that the development of

the late-stage oblique-slip faults was influenced by the presence of the older fault systems. The dominance of the NE trending System 5 faults probably reflects the development of large-scale faults associated with regional NW-SE extension.

4) From these observations, it is inferred that the heterogeneous nature of faulting in the sandstone is controlled primarily by reactivation of weak basement discontinuities. Alternatively, associating the diversity of fault orientations and timing to multiple reorientations of stresses, ignores the potential influence of pre-fractured basement at shallow crustal conditions.

5) Fracturing post-dates faulting. The distribution and orientation of some fractures mirror older fault systems in the sandstone and may also be controlled by pre-existing basement discontinuities. Fracture trends in the sandstone mirror fracture trends in adjacent basement outcrops and fractures are often spatially associated with faults. The formation of fractures in the sandstone may be related to the response of basement to stress release during erosion.

6) This part of the study provides important insight into the nature of deformation in and near the basement in an area not influenced or overprinted by the effects of large-scale faulting. Movement along numerous, diversely oriented discontinuities in the basement accommodates local variations in the strain field while the large-scale normal faults accommodate regional extension.

The detailed study of secondary faults formed between an echelon, oblique-slip faults, leads to the following general observations and conclusions:

1) The distinctive arrangement of faults that characterizes the secondary-fault zones (SFZ) observed in the Llano River outcrop (Figure 15) is a common attribute of fault systems where the bounding faults overlap and step opposite to their sense of shear. The geometry is best observed when the plane of observation is nearly parallel to the slip vector and perpendicular to the planes of the bounding faults. These features have been identified in all structural settings, in various laboratory experiments and are developed in various materials under conditions in which faulting is the dominant deformation mechanism. The geometry is readily overprinted as the fault zone evolves beyond the incipient stages of faulting.

2) Dimensional data of SFZ, from this and other studies, indicate that these features are generally scale independent. Length (l) to width (w) ratios average between 3:1 and 4:1. Distinguishing the limited data in this study on the basis of initial overlap and effective overlap suggests that SFZ may have a scale dependent nature as they develop with continued displacement. Field observations indicate that some minimum overlap between the bounding faults (critical l/w on the order of 1.5 to 1) is necessary for the development of antithetic faults that link the bounding faults. Maximum l/w values are on the order of 5:1 to 6.5:1.

3) Measurements of the acute angle between bounding faults and associated antithetic faults (α), in the SFZ developed in the Hickory Sandstone, range between 12° and 62° (average α approximately 37°). This contrasts sharply with observations from other examples of SFZ that have α values consistently in the range of 60° . Observations from this study suggest that α may systematically increase with decreasing spacing between bounding faults, however, the significance of the wide variation in values of α are not fully understood at present.

4) Observations indicate that displacements on bounding faults in the overlap region are not uniform. Changes in displacements along a bounding fault are inferred to be step-like and are directly associated with abutting, antithetic faults. The corresponding displacements on antithetic faults apparently are uniform. Displacements at the ends of bounding faults can be finite where they form Tips with associated antithetic faults. Also, the magnitudes of offset on some secondary faults are disproportionately large with respect to their lengths. Large offsets on "short" secondary faults are possible because of the kinematic and spatial relationships between bounding and associated antithetic faults.

Additional observations and conclusions on the nature of secondary-fault zones, expressed in the form of a model of SFZ evolution, are illustrated in Figure 33 and outlined below:

1) The bounding, primary faults are configured so that they step opposite to their sense of shear. These faults would tend to lengthen

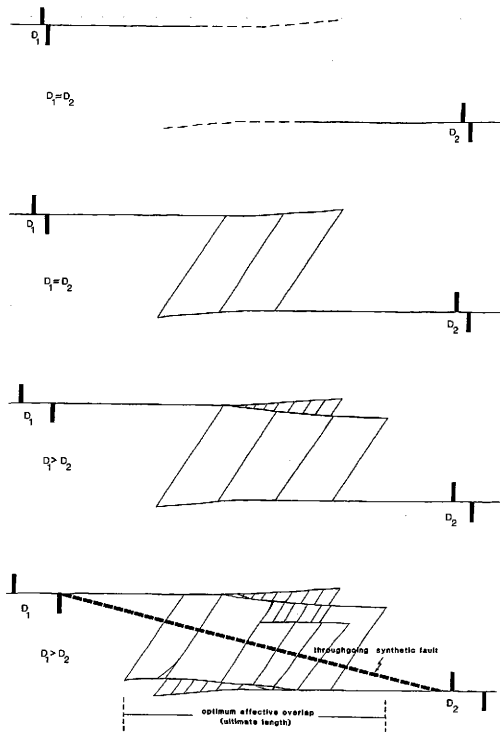


Figure 33. Generalized model of Secondary-Fault Zone evolution.

in plane (or nearly in plane) due to the nature of fault interaction, thus achieving some initial overlap.

2) With continued displacement on the bounding faults, a set of first order, antithetic faults form in response to induced stresses in the overlap region (forming the Elementary SFZ geometry). The antithetic faults mechanically link the bounding faults, forming a longer, effectively continuous fault. If the additional displacement on the bounding faults is completely transferred through the antithetics, no further secondary faulting is required (d_1 , remains approximately equal to d_2 in Figure 33b).

3) Continued displacement generates a synthetic fault and an associated subsystem of antithetic faults (forming the Compound SFZ geometry). The synthetic fault forms ahead of and toward the interior of the overlap region, thus increasing the effective overlap and decreasing the step between interacting fault pairs. The primary fault, with which the synthetic fault is associated, has more displacement than the other primary fault, illustrating a case where the additional displacement is not totally transferred through the secondary faults (d_1 , not equal to d_2 in Figure 33c).

4) Additional interaction, due to continued displacement, generates higher order synthetic and associated antithetic faults (evolving to the complex Compound SFZ geometry). If the SFZ lengthens to an optimum effective overlap, younger synthetic faults continue to reduce the space between interacting fault pairs but do not continue to form ahead of the zone.

5) If the optimum effective overlap is reached and additional transfer of displacement through the secondary faults is required, then throughgoing synthetic faults may be generated, directly linking the bounding faults (SFZ evolves to the Advanced geometry). In general, the fault zone develops so that displacements are transferred through the most efficient route through the SFZ; ultimately the sharp step between the en echelon faults is smoothed into a "ramp".

This study provides previously undocumented information on the kinematic and spatial relationships between primary and secondary faults and between antithetic and synthetic faults. Field observations support the interpretation that the role of secondary faults, formed between en echelon faults that step opposite to their sense of shear, is to accommodate displacement transfer across the overlap region. Additionally, this study provides insight into the potential sequence of fault zone development, prior to being overprinted by deformation associated with large-scale faulting.

REFERENCES CITED

- Andreason, G. E., and Petrafeso, F., 1963, Aeromagnetic map of the Llano uplift Mason-Burnet area, central Texas: U.S. Geological Survey, Geophysical Investigations Map GP-417.
- Aydin, A., 1978, Small faults formed as deformation bands in sandstone: Pure Applied Geophysics, v. 116, p. 913-930.
- Aydin, A., and Nur, A., 1983, Evolution of pull-apart basins and their scale independence: Tectonics, v. 1, p. 91-105.
- Aydin, A., Schultz, R. A., and Pollard, D. D., 1985, Why do strike-slip faults overlap?: EOS, Transactions, American Geophysical Union, v. 66, p. 1067.
- Barnes, V. E., 1981, Llano sheet, geologic atlas of Texas: Univ. of Texas (Austin), Bureau of Economic Geology, map.
- Barnes, V. E., and Bell, W. C., 1977, The Moore Hollow Group of central Texas: Univ. of Texas (Austin), Bureau of Economic Geology Report of Investigations No. 88, 169 p.
- Bartlett, W., 1980, Experimental wrench faulting at confining pressure (M.S. thesis): College Station, Texas A&M Univ., 98 p.
- Becker, J. E., 1985, Structural analysis of the western Llano Uplift with emphasis on the Mason fault (M.S. thesis): College Station, Texas A&M Univ., 203 p.
- Borg, I., and Handin, J., 1966, Experimental deformation of crystalline rocks: Tectonophysics, v. 3, p. 249-398.
- Boyer, R. E., Clabaugh, S. E., Gates, C. H., and Moffett, J. R., 1964, Comparison of two joint study methods applied to the Red Mountain Gneiss, Llano County, Texas: Texas Journal of Science, v. 18, p. 478-486.
- Cheney, M. G., and Goss, L. F., 1952, Tectonics of central Texas: American Association of Petroleum Geologists Bulletin, v. 36, p. 2237-2265.
- Fisher, N. E., 1960, Geology of the Hilda-Northwest area, Mason County, Texas (M.S. thesis): College Station, Texas A&M Univ., 73 p.
- Friedman, M., and Shimamoto, T., 1978, Fracture patterns in simulated fault gouge: EOS, Transactions, American Geophysical Union, v. 59, p. 1208.

- Gay, N. C., and Ortlepp, W. D., 1979, Anatomy of a mining-induced fault zone: Geological Society of America Bulletin, v. 90, p. 47-58.
- Groshong, R. H., Jr., 1967, Geology and fracture patterns of north-central Burnet County, Texas (M.A. thesis): Austin, Univ. of Texas, 81 p.
- Heald, M. T., 1956, Cementation of Simpson and St. Peter sandstones in parts of Oklahoma, Arkansas and Missouri: Geology, v. 64, p. 16-30.
- Hutchinson, R. M., 1956, Structure and petrology of the Enchanted Rock batholith, Llano and Gillespie Counties, Texas: Geologic Society of America Bulletin, v. 67, p. 763-806.
- Iranpanah, A., 1964, Structural geology of Burnet area, Burnet County, Texas (M.A. thesis): Austin, Univ. of Texas, 83 p.
- Jamison, W. R., 1979, Laramide deformation of the Wingate Sandstone, Colorado National Monument (Ph.D. dissertation): College Station, Texas A&M Univ., 170 p.
- Johnson, B., and Becker, J., 1986, Normal fault development in the western Llano Uplift of central Texas: Geological Society of America Bulletin, Abstracts with Programs, v. 18, p. 646.
- McGarr, A., Pollard, D. D., Gay, N. C., and Ortlepp, W. D., 1979, Observations and analysis of structures in exhumed mine-induced faults: In Proceedings of Conference VIII: Analysis of Actual Fault Zones in Bedrock, U.S. Geological Survey Open File Report 79-1239, p. 101-120.
- Patton, T. L., 1984, Normal fault and fold development in sedimentary rocks above a pre-existing basement normal fault (Ph.D. dissertation): College Station, Texas A&M Univ., 99 p.
- Pittman, E. D., 1981, Effect of fault-related granulation on porosity and permeability of quartz sandstones, Simpson Group (Ordovician), Oklahoma: American Association of Petroleum Geologists Bulletin, v. 65, p. 2381-2387.
- Schmittle, J. M., 1987, Deformation bands as a mechanism of cataclastic deformation in the Llano Uplift, Mason County, Texas (M.S. thesis): College Station, Texas A&M Univ.
- Segall, P., and Pollard, D. D., 1980, The mechanics of discontinuous faults: Journal of Geophysical Research, v. 85, p. 4337-4350.

- Segall, P., and Pollard, D. D., 1983, Nucleation and growth of strike slip faults in granite: *Journal of Geophysical Research*, v. 88, p. 555-568.
- Tchalenko, J. S., 1970, Similarities between shear zones of different magnitudes: *Geological Society of America Bulletin*, v. 81, p. 1625-1640.
- Wilcox, R. E., Harding, T. P., and Seely, D. R., 1973, Basic wrench tectonics: *American Association of Petroleum Geologists Bulletin*, v. 57, p. 74-96.
- Wilson, G. J., 1957, Geology of the big bend of the Llano river area, Mason County, Texas (M.S. Thesis): College Station, Texas A&M Univ., 101 p.
- Young, S. R., 1982, Characterization of and parameters controlling small faults in naturally deformed, porous sandstones (M.S. thesis): College Station, Texas A&M Univ., 118 p.

VITA

NAME: Howard Reiffert Hedgcoxe
BIRTHDATE: August 3, 1960
BIRTHPLACE: Albuquerque, New Mexico
FAMILY: Wife, Anne McCauley Hedgcoxe
Daughter, Clair Anne Hedgcoxe
EDUCATION: Texas A&M University
B.S., Geology, 1983

WORK EXPERIENCE IN GEOLOGY:

May 1984-May 1985: Graduate Teaching Assistant
Department of Geology
Texas A&M University
College Station, Texas

Present: Geologist
ERM Southwest, Inc.
Houston, Texas

ADDRESS: Center for Tectonophysics
Texas A&M University
College Station, Texas 77843